

Tailed Radio Galaxies from the TIFR GMRT Sky Survey

Netai Bhukta¹, Sushanta K. Mondal¹, Sabyasachi Pal^{2*}

¹*Department of Physics, Sidho Kanho Birsha University, Ranchi Road, Purulia 723104, India*

²*Indian Centre for Space Physics, 43-Chalantika, Garia Station Road, Kolkata 700084, India*

Accepted XXX. Received YYY; in original form ZZZ

ABSTRACT

We present a list of candidate tailed radio galaxies using the TIFR GMRT Sky Survey Alternative Data Release 1 (TGSS ADR1) at 150 MHz. We have visually examined 5336 image fields and found 264 candidates for the tailed galaxy. Tailed radio galaxies are classified as Wide Angle Tailed (WAT) galaxies and Narrow-Angle Tailed (NAT) galaxies, based on the angle between the two jets of the galaxy. We found a sample of tailed radio galaxies which includes 203 ‘WAT’ and 61 ‘NAT’ type sources. These newly identified tailed sources are significant additions to the list of known tailed radio galaxies. The source morphology and luminosity features of the different candidate galaxies and their optical identifications are presented in the paper. Other radio properties and general features of the sources are also discussed.

Key words: galaxies: active – galaxies: formation – galaxies: jets – galaxies: kinematics and dynamics– radio continuum: galaxies

1 INTRODUCTION

Tailed radio galaxies are galaxies having a pair of radio “tails” extended far from the optical galaxy. The radio “tails” are nothing but the bending of both of the radio jets in the same direction. Initially, they are well-collimated on a kiloparsec scale and suddenly flare into diffuse plumes, which may be significantly bent (Missaglia et al. 2019; Patra et al. 2019). The spectral index of tailed radio galaxies becomes steeper moving outwards towards the tail from the core and varies from region to region (Bridle et al. 1981; Hardcastle et al. 2003; Patra et al. 2019). Most tailed radio galaxies are Fanaroff–Riley I radio galaxies (Fanaroff & Riley 1974), where the surface brightness is relatively higher towards the end of the jets than the regions close to the core (Terni de Gregory et al. 2017; Missaglia et al. 2019). Tailed radio galaxies are distinguished by their radio morphology, which includes bright hotspots (called “warmspots”) that are closer to their radio core than FR IIs (Missaglia et al. 2019). Tailed sources are classified depending on the angle between the radio tails and the core of the galaxy. The narrow-angle tail (NAT) radio sources are featured by tails bent in a narrow ‘V’ or ‘L’ shape where the angle between two tails is less than 90 degrees. The jet bending in the case of Wide-angle tail (WAT) radio sources is such that the WATs exhibit wide ‘C’ type morphologies and the angle between the two components is greater than 90 degrees but less than 180 degrees. These ‘WAT’ and ‘NAT’ morphologies were first defined in Owen & Rudnick (1976). The structures of NAT sources may be affected by the projection effect. The luminosity of the

WAT sources comes in between the classical double and the NAT sources (O’Donoghue et al. 1993).

Tailed sources are generally found in the dynamical, active, and X-ray intense regions of the rich clusters (Burns 1981; O’Dea & Owen 1985). It is considered that the ram pressure associated with the dynamical interaction of the host galaxy with the dense intercluster medium (ICM; assumed to be at rest) causes the radio jets to bend in the reverse direction of motion, away from the cluster centre (Begelman, Rees & Blandford 1979; Vallee, Bridle & Wilson 1981; Baan & McKee 1985). The degree of bending depends on the velocity of the host galaxies (Srivastava & Singhal 2020). The NAT sources are found towards the edge of the associated cluster, while the WAT sources are generally found close to the gravitational centre of the clusters (Quintana & Lawrie 1982). The ram pressure explanation of jet bending does not hold for the WAT sources as they move very slowly compared to the NATs (Burns & Balonek 1982). The WAT morphology is believed to cause by strong intercluster wind (Burns et al. 1986), in some literature it is attributed to the electromagnetic interaction of the non-neutral jet with the ICM magnetic field (Eilek et al. 1984).

Tailed radio sources can be used to trace galaxy clusters and high redshift systems (Blanton et al. 2000, 2001; Smolcic et al. 2007); to investigate the inner cluster environment (Douglas et al. 2011; Wing & Blanton 2011; Blanton et al. 2001); to study the cluster magnetic field (Feretti et al. 1999); to study the interaction of the jet with the intercluster medium and to study the evolution of galaxies and galactic dynamics (Pinkney et al. 1992). The tailed radio galaxies are normally representatives of Fanaroff & Riley (1974) class I sources, but in terms of luminosities, one

* E-mail: sabya.pal@gmail.com

can place them close to the FR II transition (Miley et al. 1972; Bliton et al. 1988). However, on a scale of arcseconds, these tailed galaxies normally have U-shaped symmetry constructed by a pair of bent jets which originate from the nucleus and meet with the more elongated tails after adequate bending (Owen, Burns and Rudnick 1979; O’Dea & Owen 1986). So far, most of the tailed galaxies have been discovered entirely in galaxy clusters, with the majority of them being rich galaxy clusters (Mao et al. 2009). At least a few factors influence the bending of tailed radio galaxies. (1) Most of the tailed radio galaxy search activities focus on galaxies in clusters (O’Dea & Owen 1985) and the bending of radio tails is due to the motion of the host galaxy through the inter-cluster medium. (2) The hypotheses that host galaxy orbits are either radial, circular, or isotropic (Jones & Owen 1979) are tested using the initial ejection angle of the jet with respect to the motion of the galaxy and the jet flow velocity (Baan & McKee 1985). (3) The differences in the ejection of jets with respect to the direction of motion of the host galaxy in the inter-cluster medium and environments, as well as projection effects, are responsible for the asymmetries found in the radio jets in some tailed radio galaxies (Sebastian et al. 2017). (4) The probability of detection of tailed radio sources decreases in the clusters with less number of galaxies (Stoche 1977; Adams, Jensen & Stoche 1980). (5) Various types of bending may be caused by precessing radio jets. Due to projection effects, the distinction between WATs and NATs is somewhat arbitrary. Many of the WAT sources look like NAT sources simply due to projection effects. Transonic or supersonic relative motions drive the jets of tailed radio galaxies. Even with high-resolution (arcsec scale) radio observations, a few NAT sources have been discovered to have a remarkable narrow extended structure, with the two radio tails not being resolved (e.g. IC 310; Feretti et al. (1988)).

WATs display bending of two jets less than NATs, and the bending model of dynamical ram pressure can not completely explain the bending of WATs morphology (Burns 1981; Burns et al. 1982; Eilek et al. 1984). WAT sources appear to be associated with large size D or cD galaxies approaching rest at cluster centres (e.g., 3C 465) and therefore should not have the necessary velocity to produce the ram pressure required for the observed bends in their radio jets. So, an alternative fundamental mechanism is required to interpret the noticed bending of jets of WATs. An electromagnetic force that results from the interaction of a jet carrying a net electrical current with the magnetic field of the inter-cluster medium may be responsible for the bending of jets in WATs (Eilek et al. 1984). An ordered magnetic field is required to generate the symmetric shape of WATs. Collisions with dense clouds in the ICM, on the other hand, may also deflect jets. In some WATs, this method may be responsible (Burns et al. 1986) but it is difficult to reproduce the large-scale symmetric structure of WATs by only this method.

The tailed radio galaxies are normally representatives of Fanaroff & Riley (1974) class I sources, but in terms of luminosities, one can place them close to the FR II transition (Miley et al. 1972; Bliton et al. 1988). However, on a scale of arcseconds, these tailed galaxies normally have U-shaped symmetry constructed by a pair of bent jets which originate from the nucleus and meet with the more elongated tails after adequate bending (Owen, Burns and Rudnick 1979; O’Dea & Owen 1986). So far, most of the tailed galaxies have

been discovered entirely in clusters, with the majority of them being rich clusters (Mao et al. 2009).

O’Dea & Owen (1985) has identified 57 tailed sources in the directions of different clusters using the A and B configurations of the VLA at 20 cm. This sample of 57 sources includes 41 NATs, 9 WATs and 7 sources with complex morphologies. O’Donghue, Owen & Eilek (1990) identified 11 WATs in 20 cm using VLA in A and C configuration. Detail study of big WAT 1919+479 is presented in Piffaretti et al. (1998). Six other WATs are found in the ATLAS field at 1.4 GHz using ATCA (Mao et al. 2010). NGC 1265 is a well studied NAT source (Xu, O’Dea & Biretta 1999). Around 1600 sources are identified as possible ‘tailed’ candidates using a pattern recognition algorithm (Proctor 2016) using the NRAO VLA Sky Survey (NVSS; Condon et al. (1990)) at 1.4 GHz. In this paper, we present 264 tailed radio sources of which 198 sources are located in the northern sky (above 0 degrees). We have classified 203 sources as ‘WAT’ type and 61 sources as ‘NAT’ type based on the angle made by the two bent lobes. Most of these sources have been observed before and catalogued in different radio surveys, mostly in the NVSS survey and in the Sydney University Molonglo Sky Survey (SUMSS; Mauch et al. (2003)) at 843 MHz, but have not been reported as tailed sources. We found that only about half of the sources are associated with a known galaxy cluster. The optical galaxy hosting the radio sources is located in the redshift range of 0.01 to 0.68 and the total flux at 150 MHz ranges from 0.1 Jy to as large as 20.1 Jy. Redshifts are found for 165 WATs out of 203 detected optical/IR counterparts (75 per cent). For NATs, redshifts are found for 49 galaxies out of 61 detected optical/IR counterparts (76 per cent). Out of 117 identified redshifts of tailed radio galaxies, fifty are identified spectroscopically. We arrange the paper in the following ways: In section 2, we present the method of the identification of sources. We describe the counterpart identification in section 3. In the next section (section 4), we describe the different radio properties of the sources. In section 5, we discuss the general features and overall properties of sources. We summarise the study in the final section. We assumed the flat Λ CDM cosmology with $H_0 = 67.8 \text{ km s}^{-1} \text{ Mpc}^{-1}$, $\Omega_M = 0.308$, and $\Omega_\Lambda = 0.692$ (Aghanim et al. 2018).

2 IDENTIFICATION OF TAILED-RADIO GALAXIES

2.1 The TGSS alternative data release one

The tailed sources are found from the manual inspection of a large number of high-resolution images generated by the TIFR GMRT Sky Survey Alternative Data Release 1 (TGSS ADR 1; Intema et al. (2017)). The continuum survey at 150 MHz using the Giant Metrewave Radio Telescope (GMRT; Swarup (1991)) covers a declination range from -55 to $+90$ degrees. The purpose of the survey was to provide a high-resolution and high sensitivity map of the 150 MHz sky. The median noise of the survey is $3.5 \text{ mJy beam}^{-1}$ and the resolution is $25'' \times 25''$ north of 19° DEC and $25'' \times 25'' / \cos(\text{DEC} - 19^\circ)$ south of 19° . In total, over 2000 hours of observation time were used over about 200 observing sessions. Earlier, four tailed galaxies were serendipitously discovered with GMRT at 610 and 327 MHz (Giacintucci & Venturi

2009). Detection of a WAT (J0037+18) with an interacting host galaxy as optical counterpart (Patra et al. 2019) is reported in the same frequency bands using GMRT.

2.2 Definition of WAT and NAT

WATs are usually irregular radio galaxies with bright hotspots (known also as warm-spots with respect to FR-II) settled with host clusters, and their relative rest frame velocities are low ($< 1000 \text{ km s}^{-1}$). Twins of well-collimated radio jets make obtuse bending angles (≥ 90 degrees) under the influence of ICM weather/wind or induced merger shocks. In the 3C catalogue, WAT-3C 465 is known as its prototype (Burns 1981; Eilek et al. 1984; Eilek & Owen 2002; Hardcastle et al. 2005). Because two tails are bent in the same direction, it is probably implied that the intra-cluster environment should have some regular ICM motion relative to the jets, rather than turbulence motion. We have included a source in our WAT sample if the bending angle is less than 160 degrees and if the source follows the selection criterion mentioned in subsection 2.3.

NATs are common in clusters, usually moving at high speeds through their central clusters ($\geq 2000 \text{ km s}^{-1}$; Huchra et al. (1999); Sun et al. (2005)), and their distinctive structures reveal strong interactions with the inter-cluster medium, with radio tails bent in the same direction as core galaxies.

2.3 Search from TGSS ADR 1

We have made use of the TGSS ADR 1 consisting of images of a total of 5536 fields with a typical noise of $\sim 5 \text{ mJy}$ at 150 MHz. The observations corresponding to this data release were executed between 2010 and early 2012 and cover about 90 percent of the whole sky. The survey covers 1 steradian of the southern sky, the maximum accessible southern sky from the observatory location. In search of tailed radio galaxies, we closely examine each of these 5536 image fields using Astronomical Imaging Processing Software (AIPS). The good sensitivity and high resolution of TGSS (average rms of $3.5 \text{ mJy beam}^{-1}$) helps to study new fainter samples of different types of radio galaxies, such as X-Z shaped radio galaxies (Bhukta et al. 2020), and giant radio galaxies (Bhukta et al. 2021). We visually examined all 5536 fields of TGSS images. For the selection of tailed radio source samples from TGSS, we tried the rigorous and tedious way and checked each of 5536 fields manually. Our source selection criteria are as follows:

1. To make an initial list of probable WATs and NATs we make a list of radio sources showing two-sided jets with a clear bending angle ≤ 160 degrees.

2. The majority of tailed radio sources show a bright radio centre near host galaxies, which is known as ‘‘head’’. So, we go through all probable tailed radio sources to check if there is any bright source near the radio core location. To ensure radio core positions, we also compute the spectral index near the host galaxy and check whether the corresponding spectral index is flat. This radio core position is indicated as the cross mark.

3. For WAT/NAT sources, radio jets extend into plumes beyond the radio head. We identify sources with warmspots

near both sides of the radio head. We measure the peak flux of warmspots of probable WAT/NAT sources, which should be higher than the tail radio flux.

4. We measure the angle between the two tails of all radio sources with the radio core. If the angle of the sources is greater than 90 degrees, then the source is catalogued as WAT, and if the angle is ≤ 90 degrees, the source is named as NAT.

5. All selected sources have a greater angular size than the synthesised beam (~ 4).

In figure 1, we present the above mentioned criteria of an ideal radio image of tailed radio sources with surface brightness contours from TGSS, FIRST, and NVSS radio maps.

We excluded 20 bent sources from our list as they may be radio relics of a cluster. These possible relics are chosen using the following criterion.

1. These diffuse and bent sources are located within 20 kpc of the position of the centre of a known galaxy cluster.

2. There are no optical/IR counterparts or radio cores in these sources. They also lack any warm-spots.

3. We study multi-wavelength radio images of these diffuse radio sources.

4. The power law radio spectrum is steeper ($\alpha \sim 1.2 - 1.3$).

Similar studies of tailed radio sources were recently conducted using a variety of methodologies. Double radio sources were found with different morphological radio sources (15 types) via automated pattern recognition using NVSS (Proctor 2011). In this catalogue, 199 C-shaped radio galaxies (either WATs or NATs) were present. From the Proctor sample, Yu-Xing et al. (2019) confirmed 412 C-shaped sources.

The sample of detected WATs/NATs is flux limited and not complete as the detection depends on the lower contour of each image. It is complete upto $10.2 \text{ mJy beam}^{-1}$.

3 COUNTERPART IDENTIFICATION

This section focuses on the identification of the optical and IR counterparts of the tailed radio sources. We use a likelihood ratio (LR) technique that is particularly useful when dealing with deep optical images to minimise the number of spurious associations. For 261 of our tailed radio sources, we find a reliable counterpart.

3.1 Likelihood ratio technique

The Likelihood ratio technique (LR; Richter (1975); de Ruiter et al. (1977); Sutherland & Saunders (1992); Ciliegi et al. (2003)) method allows us to take into account not only the position of the counterpart but also the background source magnitude distribution and the presence of multiple possible counterparts for the same radio source. It is given by the relationship (Sutherland & Saunders 1992)

$$LR = \frac{q(m)f(r)}{n(m)} \quad (1)$$

$n(m)$ represents the surface density of background sources as a function of band magnitude m . This surface density is defined as the ratio of the magnitude distribution of background sources to the total searching area. The parameter $q(m)$ represents the *a priori* probability that the radio source

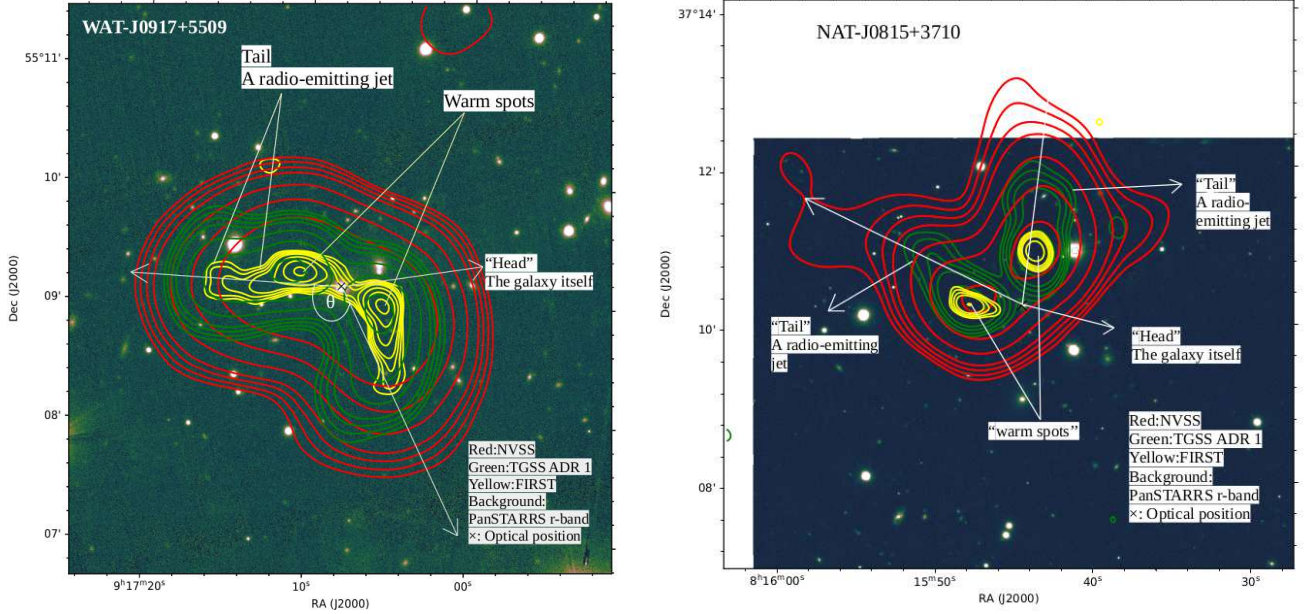


Figure 1. A figure shows an example of ideal WAT (left) and NAT (right) sources. PanSTARRS r-band optical images are overlaid with TGSS, NVSS, and FIRST images. In both of the images, contour levels are at $3\sigma \times [-1, 1, 1.4, 2.0, 2.8, 5.6, 11.2, 22.4]$, where σ for the TGSS, FIRST, and NVSS are 3.5, 0.15, and 0.45 mJy beam⁻¹, respectively. Both tailed radio sources are associated with host galaxies or radio cores (known as “Head”) that are indicated as cross marks. A pair of bright hotspots (called “warmspots”) are located closer to their radio core with respect to FR-II. The surface brightness is relatively higher towards the end of the jets than in the regions close to the core. Beyond these warmspots, well-collimated jets suddenly flare into diffuse plumes that may be significantly bent (known as “Tails”). For the WAT, the angle (θ) between two tails of the radio galaxy is $90 \leq \theta \leq 180$ degrees, and for NAT, the angle is ≤ 90 degrees.

has a counterpart of magnitude m . According to Ciliegi et al. (2003), the parameter $q(m)$ is derived from

$$q(m) = \frac{\text{real}(m) \times Q}{\sum_{m_i} \text{real}(m_i)} \quad (2)$$

The $\text{real}(m)$ is calculated from the following equation.

$$\text{real}(m) = \text{total}(m) - n(m) \times N_{\text{radio}} \times \pi r_{\text{max}}^2 \quad (3)$$

where N_{radio} is the number of radio sources in the catalogue, $\text{total}(m)$ is the objects in the subsidiary catalogue within a radius of r_{max} ($\sim 2''$) around each radio source and the Q is usually estimated by determining the fraction of sources with radio counterparts above the background as follows:

$$Q = \frac{N_{\text{counterparts}} - (\sum_{m_i} n(m) \times r_{\text{max}}^2 \times N_{\text{radio}})}{N_{\text{radio}}} \quad (4)$$

The parameter $f(r)$ represents the probability distribution of the off-set r between the catalogued positions of the radio source and its potential counterpart. The uncertainty in this offset is calculated by combining the uncertainty in the radio position, the uncertainty in the optical/IR position, and the uncertainty in the relative astrometry of the two surveys. As for $f(r)$, we adopt a two-dimensional Gaussian distribution of the form:

$$f(r) = \frac{1}{2\pi\sigma^2} \exp\left(-\frac{r^2}{2\sigma^2}\right) \quad (5)$$

For each source, σ is the average value between $\sigma_x = \sqrt{er_{\text{op}}^2 + \sigma_\alpha^2}$ and $\sigma_y = \sqrt{er_{\text{op}}^2 + \sigma_\delta^2}$, where er_{op} is the position error of the counterpart and σ_α and σ_δ are the radio positional errors in RA and DEC. The LR does not contain information about the possible presence of many counterpart

candidates in the surrounding of a specific radio source. It is therefore useful to define the reliability of each association as:

$$\rho_j = \frac{(LR)_j}{\sum_i (LR)_i + (1 - Q)} \quad (6)$$

where the sum is over all the candidate counterparts for the same radio source (Sutherland & Saunders 1992).

3.2 Subsidiary catalogue of WISE and Pan-STARRS data

The selection of multi-wavelength data is crucial to identify the correct counterpart of a radio source. We use two deep optical surveys from the Panoramic Survey Telescope and Rapid Response System (Pan-STARRS; Chambers et al. (2016)) and infrared survey from the Wide-field Infrared Survey Explorer (WISE; Wright et al. (2010)). Deep and wide optical and IR data are available over the TGSS-ADR 1 covered sky. Pan-STARRS1 has performed a set of independent synoptic imaging sky surveys, including the 3π steradian survey. This survey covers the entire northern sky and southern sky upto $\delta > -30$ degrees. There are five bands present *grizy* (23.3, 23.2, 23.1, 22.3, 21.4 mag). The typical point spread function (PSF) of the Pan-STARRS images is $\sim 1 - 1.3''$. In the astrometric calibration, the uncertainty of the standard deviation of the mean and median residuals ($\Delta\alpha$, Δdec) are (2.3, 1.7) milliarcsec and (3.1, 4.8) milliarcsec, respectively. The WISE covers a mid-infrared survey of the entire sky. The sensitivity of this survey is much higher than previous infrared survey missions. WISE achieved a sensi-

tivity more than 100 times better than IRAS in the 12 μm band. WISE is covering the whole sky in four infrared bands W1, W2, W3, and W4 in the 3.4, 4.6, 12, and 22 μm respectively. The All WISE catalogue includes more than 747 million sources across the full sky. The W1 and W2 bands have significantly better sensitivity than the other two WISE bands (Cutri et al. 2013). The completeness of the WISE catalogue varies across the sky. With $W1 < 19.8$, $W2 < 19.0$, $W3 < 16.67$, and $W4 < 14.32$ mag, the completeness is 95 per cent for sources. Initially, we included all WISE sources smaller than $15''$. The WISE W1-band and Pan-STARRS i -band data sets are combined using LR band magnitude analysis. For each WISE source, we searched for the best Pan-STARRS match in i band. LR ratios are then derived for all PanSTARRS sources within $15''$ of all WISE position. And for each WISE source, the highest LR above the threshold limit is taken as the PanSTARRS counterpart. Finally, we make a WISE-Pan-STARRS combined catalogue that should be used for counterpart identification.

3.3 Cross-match of tailed radio sources with subsidiary catalogues

We use the magnitude and colour in the LR method to cross-match the TGSS ADR1 tailed radio sources with the subsidiary WISE-Pan-STARRS combined catalogue. Following the LR method, we built a list of possible counterparts for each of the tailed radio sources. Initially, we set a very low likelihood threshold to be sure not to lose any counterparts. After a careful analysis, we select only those sources with a reliability greater than 0.6, as the threshold limit to ensure the expected number of spurious associations is 4 per cent of the subsidiary catalogue. As a result, maximising the number of identified tailed radio sources was maximised. Another approach to measuring a value for the reliability limit, where those sources with a reliability greater than ρ_c can be accepted as true counterparts, was done by Smith et al. 2011. They estimated the number of false cross-matches using $N_{false} = \sum_{\rho \geq 0.8} (1 - \rho)$ and determined the contamination rate ~ 4.2 (ratio of N_{false} to matched sources with reliability limit). In our catalogue, the number of N_{false} is 12 and matched sources with reliability limit is 261. The contamination rate is 4.5 per cent with the reliability limit of 0.6 using the above relation.

The choice of the best threshold value LR_{thr} is necessary to discriminate between spurious and real identifications. Here, LR_{thr} should be large enough to keep the number of spurious identifications as low as possible and to increase the reliability. We defined a source as counterparts tailed radio sources if their LRs are above the thresholds of $LR_{thr} = 7.57$ in the i -band or $LR_{thr} = 0.77$ in the W1-band. If more than one spurious counterpart is above those thresholds, then the counterpart with the highest LR in either of the two bands is accepted and the other is discarded. The counterpart identification rates in our catalogue are 61 per cent and 98 per cent in the i and W1 bands, respectively. We also calculate the radio optical separation of each radio source with the highest reliability. The distribution of radio optical separation is shown in Table 1 and Table 2. With this criteria, a 3 per cent counterpart (8/261) is identified with spurious associa-

tion. Figure 3 presents the distribution of separation between optical and radio counterparts. A peak is seen near 4 arcsec.

We make use of other previous all-sky surveys. In particular, we use the SDSS DR-12 catalogue (Alam et al. 2015) and the Two Micron All Sky Survey (2MASS; Skrutskie et al. 2006) extended source catalogue (2MASX; Jarrett et al. 2000). We found the optical counterparts of 57 WATs in SDSS, 26 in the 2MASS catalogue, and 13 in the 2MASX catalogue, respectively. We also identify optical counterparts for 10 NATs in SDSS, 11 in the 2MASS catalogue, and 17 in the 2MASX catalogue, respectively. In our catalogue, about 117 tailed radio galaxies (92 WATs and 25 NATs) have redshift information. For 92 WATs, the spectroscopic redshift data that can be collected from the SDSS is 34, for NATs it is three. Since optical/IR counterparts are more compact than the corresponding radio galaxies, we used the position of optical/IR counterparts as the position of these sources. For the rest of the 4 (1 per cent of total detected sources) tailed radio sources, where optical or IR counterparts are not available, a radio-morphology based position is used.

By visual search, Dehghan et al. (2014) detected 56 bent tailed radio sources over ~ 4 square degrees area of the southern sky in the ATLAS field. From combined mosaic radio sources (FR-I and FR-II) of the southern sky, new 24 bent tailed samples were identified by visual inspection (O'Brien et al. 2018). Missaglia et al. (2019) presented a catalogue of 47 wide-angle tailed radio galaxies (WATs). All candidates were selected by combining observations from the NVSS, FIRST, and SDSS surveys. With the help of the VLA FIRST survey at 1.4 GHz, Pal & Kumari (2021a) found 614 new head-tail radio galaxies, among them, 398 were WATs and 216 were NAT sources. Pal & Kumari (2021) presented a catalogue of fifty new head-tail radio sources (five NATs and forty-five WATs) using LOFAR Two-metre Sky Survey first data release (LoTSS DR1) at 144 MHz frequency (Shimwell et al. 2019). The survey coverage area of the present paper is larger than all other previous works.

4 RESULTS

Different information about the objects reported in this paper is given in Table 1 and Table 2. In the first two columns, the catalogue number and identification names are given. Columns (3) and (4) contain the J2000 coordinates of the optical/IR counterpart. The radio counterpart separation is presented in column (5). When the optical counterpart is not found, the approximate position using the morphology of the radio source is provided. The reliability of counterpart (ρ) is presented in columns (6). In columns (7) and (8), the total flux density in Jy at 150 MHz (F_{150}) and 1400 MHz (F_{1400}) obtained from the TGSS and NVSS surveys is provided. Columns (9) and (10) contain the spectral index and redshift of the sources respectively. In column (11), we provide the luminosity in 150 MHz. Column (12) contains the names of earlier radio surveys where the source is presented without identification of them as tailed radio galaxies.

We report the discovery of 203 WAT and 61 NAT sources from the TGSS ADR 1 at 150 MHz. We remove sources reported in Proctor (2011) and other catalogues from our list (Dehghan et al. 2014; Missaglia et al. 2019; Yu-Xing et al. 2019). Dehghan et al. (2014) have identified 45 bent-tailed

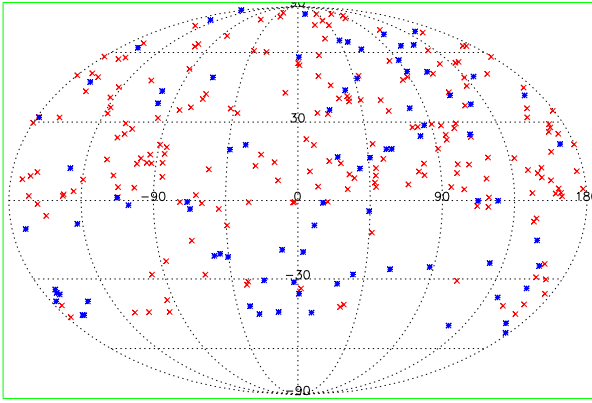


Figure 2. The spatial distribution of tailed radio sources. The ‘x’ symbols indicate WAT sources and the ‘*’ symbols represent NAT sources.

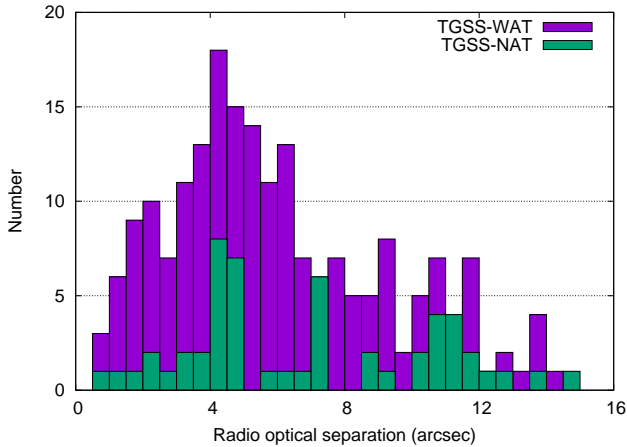


Figure 3. Distribution represent the separation between radio and optical positions of tailed radio sources.

(BT) radio galaxies in Australia Telescope Large Area Survey (ATLAS) at 1.4 GHz, which is supplemented with the 1.4 GHz Very Large Array images. Proctor (2011) identified 199 WATs or NATs radio galaxies by using an automated morphological classification scheme. Missaglia et al. (2019) presented a catalogue of 47 wide-angle tailed radio galaxies (WATs). All candidates were selected by combining observations of the NVSS survey, FIRST survey, and SDSS survey. We present the spatial distribution of the newly identified WAT and NAT sources in Figure 2. As expected, the sources show a random distribution. Many of these newly identified sources are catalogued as two separate sources in the NVSS catalogue (Condon et al. 1990). The number of sources is higher in the northern region compared to the southern region because the survey is limited up to a declination of -55 degrees and the local RMS in the southern hemisphere is higher compared to that of the northern hemisphere due to high declination effects.

We present high-sensitivity 150 MHz GMRT images of ideal selected WAT and NAT radio galaxies Figure 1 identified from the TGSS and NAT radio galaxies. We present the radio image of tailed radio sources with different contours from TGSS ADR 1, NVSS, and FIRST. PanSTARRS r-band optical images are overlaid with TGSS, NVSS, and FIRST images. In all figures, contour levels are at $3\sigma \times [-1, 1, 1.4, 2.0, 2.8, 5.6, 11.2, 22.4]$, σ for the TGSS, FIRST, and NVSS are 3.5, 0.15, and 0.45 mJy beam $^{-1}$, respectively. Overlaid images of all the tailed radio sources are available as supplementary material in the online version of the article.

4.1 Spectral index

The two-point spectral index of newly discovered radio galaxies between 150 and 1400 MHz is calculated assuming $F \propto \nu^{-\alpha}$, where α is the spectral index and F_ν is the radiative flux density at a given frequency ν . These spectral indices have been determined by integrating fluxes over the same aperture at both frequencies, using formula

$$\alpha = \frac{\log F_{\nu_1} - \log F_{\nu_2}}{\log \nu_2 - \log \nu_1} \quad (7)$$

The integrated radio flux density of tailed-radio sources can be estimated using Astronomical Imaging Processing Software (AIPS) with TVSTAT. To measure the flux density in TGSS and NVSS field, for uniformity, we use a region corresponding to the 10.5 mJy beam $^{-1}$ (3σ) contour level from TGSS.

The spectral index (α_{150}^{1400}) is mentioned in Table 1 and Table 2. For 188 WATs and 51 NATs, the spectral index measurements are available. The remaining 15 WATs and 10 NATs were not detectable in NVSS maps since their declination is less than the NVSS coverage. Out of 188 WATs with spectral index information, 13 (7 per cent) show flat spectrum ($\alpha_{150}^{1400} < 0.5$). Out of 61 NATs with spectral index information, 5 (7 per cent) are showing flat spectrum ($\alpha_{150}^{1400} < 0.5$). Most of the WATs and NATs show a steep radio spectrum ($\alpha_{150}^{1400} > 0.5$) which is a common property of lobe dominated radio galaxies. The uncertainty of spectral index measurements due to flux density uncertainty (Mahony et al. 2016) is

$$\Delta\alpha = \frac{1}{\ln \frac{\nu_1}{\nu_2}} \sqrt{\left(\frac{\Delta S_1}{S_1}\right)^2 + \left(\frac{\Delta S_2}{S_2}\right)^2} \quad (8)$$

where $F_{\nu_{1,2}}$ and $S_{1,2}$ refers to NVSS and TGSS frequencies and flux densities respectively. The flux density accuracy in TGSS ADR 1 and NVSS is ~ 10 per cent (Intema et al. 2017) and ~ 5 per cent (Condon et al. 1990). Using equation 2, the spectral index uncertainty is $\Delta\alpha=0.05$. The spectral index distribution for WATs (left) and NATs (right) with sources presented in the current article is shown in Figure 4. The distribution shows slightly different peaks for WATs and NATs. The distribution peaks near 0.6 – 0.7 for WATs and near 0.65 – 0.75 for NATs. For WAT, the total span of α_{150}^{1400} is from 0.02 to 1.86 and for NATs, the total span of α_{150}^{1400} is from 0.38 to 2.04. Among WATs, J0752+0814 has the highest spectral index (with $\alpha_{150}^{1400}=1.70$) and J0041+2104 has the lowest spectral index (with $\alpha_{150}^{1400}=0.02$). For NATs, J0704+6318 has the highest spectral index (with $\alpha_{150}^{1400}=2.04$) and J2144+2107 has the lowest spectral index (with $\alpha_{150}^{1400}=0.38$). The radio

spectral index is commonly utilised to differentiate between source components like core and lobe. To ensure the location of the core, we compute spectral index of the probable core region (found from optical/IR counterpart and radio morphology) using TGSS and FIRST survey (when available) and found that all of them are showing flat spectral index ($\alpha_{150}^{1400} < 0.5$). The spectral index of the core is shown in images of all sources, when corresponding FIRST images are available.

4.2 Luminosity feature

We have calculated the radio luminosities (L_{150}) of sources using the redshift information of either the optical counterpart or the associated galaxy cluster using the standard formula (Donoso et al. 2009)

$$L_{150} = 4\pi D_L^2 S_0 (1+z)^{\alpha-1} \quad (9)$$

where z is the redshift parameter, α is the spectral index ($S \propto \nu^{-\alpha}$), D_L is luminosity distance of the source (Mpc), and S_0 is the flux density (Jy) at 150 MHz frequency. Figure 5 shows the redshift vs luminosity plot of the 103 tailed sources for which either spectroscopic or photometric redshift is available. In our sample, the highest redshifts for the NAT and WAT sources are 0.51 and 0.68 respectively. The source radio luminosities at 150 MHz are in the order of 10^{25} W Hz $^{-1}$, which is similar to a typical radio galaxy. The average value of $\text{Log } L$ [W Hz $^{-1}$] for WATs is 25.62 (1σ standard deviation= 0.72, median= 25.63) and that of NATs is 25.82 (1σ standard deviation= 0.72, median= 25.83). J0856+4829 is the least luminous WAT in our sample with $L_{150} = 0.15 \times 10^{25}$ W Hz $^{-1}$ ($z = 0.12$) and J0549–2520 is the least luminous NAT in our sample with $L_{150} = 0.27 \times 10^{25}$ W Hz $^{-1}$ ($z = 0.04$). J0225+4031 is the most luminous WAT in our sample with $L_{150} = 1.9 \times 10^{27}$ W Hz $^{-1}$ ($z \sim 0.65$) and J1314+6220 is the most luminous NAT in our sample with $L_{150} = 162.8 \times 10^{25}$ W Hz $^{-1}$ ($z = 0.14$).

4.3 Bending angle

We measure the bending angle of all sources using the angle (2θ) between two individual jet axis connecting the core that is shown in Figure 6. We classified all tailed sources in our sample into two groups – ‘wide-angle tailed’ galaxy or ‘narrow-angle tailed’ depending on the bending angle of these sources. For some sources, the bending angle could not be measured because of the complex structure of these sources. Figure 7 presents the distribution showing the distribution of bending angles of sources presented in the current paper for both NAT and WAT type sources. Most of the NAT sources made an angle greater than 80° . WAT sources produced a wide variety of angles between the two components, with a peak near 110 – 120° .

4.4 Cluster Association

In the Universe, clusters are the greatest gravitationally bound structures (Wen et al. 2012). Clusters give an ideal tool for cosmologists to understand the composition and evolution of the structures of the Universe (Allen et al. 2011; Wetzel et al. 2012). They provide

strong proof for the appearance of large amounts (80 per cent) of dark matter (Wen et al. 2012). They are created around dark matter concentrations when two cosmic objects (sheets and filaments) are intersected. Understanding clusters is very helpful for tracing the large-scale structure of the Universe (Prestage & Peacock 1988; Hill & Lilly 1991; Worrall & Birkinshaw 2000; Belsole et al. 2007; Tasse et al. 2008). We associate our tailed radio galaxy sample with cluster catalogues from the literature that covers the TGSS field. These clusters have been detected using various methods, including optical, IR, X-ray, and SZ observations. The cluster catalogues used are listed in Table 3 and Table 4. Using only the 107 WATs and NATs candidate sources with redshifts, we performed a three-dimensional cross-match with the known clusters across the field using a search radius of 2 Mpc. The distance is computed using the source redshift. We assume that tailed-radio galaxies and clusters of galaxies are associated if $\Delta z = |z - z_{spec}| \leq 0.005$, where z_{spec} is the spectroscopic redshift of galaxy cluster (Moore et al. 1993; Eke 2004; Berlind et al. 2006). We found associated known clusters or groups for 120 tailed radio galaxies from our WATs and NATs sample (out of 264 total). The details of associated clusters for WATs and NATs presented in the current paper are listed in Table 3 and Table 4. In columns (1) and (2), the catalogue number and galaxy cluster identification name are given. In columns (3) and (4) the name of the catalogue where the cluster is named and the redshift of the cluster is given. Column (5) and (6) contains the comoving distance (D_c) in Mpc at sources redshift and angular separation (in arc) between the centre of the associated cluster and galaxy centre. Column (7) indicates the linear distance of the host galaxy from the cluster centre. In column (8), the BCG r band magnitude m_r is shown. In column (9) and (10), cluster radius (r_{500}) and cluster richness (R_L) is shown. In column (11), the number of member galaxy candidates (N_{500}) within r_{500} is shown and in column (12), the mass of the cluster within r_{500} (M_{500}) is presented. The cluster density (ρ_{co}) is presented in column (13). For a homogeneous study, various parameters (m_r , r_{200} , N_{500} , and R_L) of clusters in Table 3 and Table 4 are collected from Wen et al. (2012); Wen et al. (2015). We calculate the optical mass M_{500} and cluster density ρ_{co} using these parameters. We also found that for 65 tailed-radio sources in our sample, the distance between two sources is less than 500 kpc. Search for a new cluster of galaxies is encouraged near these WATs and NATs when no associated cluster has been identified.

5 DISCUSSION

5.1 Radio properties of WATs and NATs

Based on our study, we further discuss our results of tailed radio sources in this section. In this section, we also include other samples (WAT-CAT catalogue, LoFAR catalogue) and compare with their results.

In Figure 9, the variation of radio luminosity with the spectral index of tailed radio galaxies is shown. The figure indicates that the spectral index tends to increase with the radio power. The correlation is significant for our sample, which was selected at a low frequency of 150 MHz. This result is consistent with previous studies (Blundell et al.

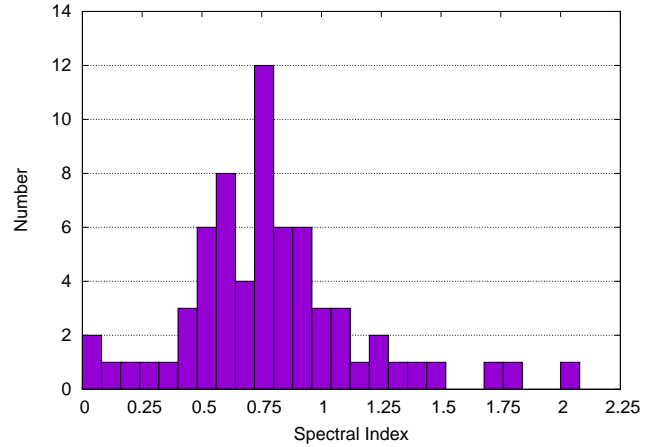
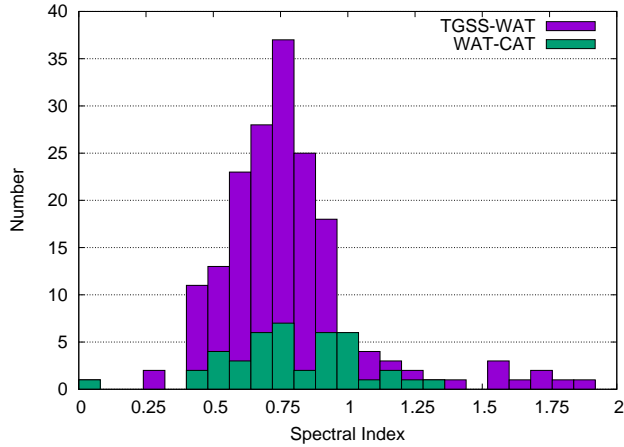


Figure 4. Distribution showing spectral index distribution for WAT (left) and NAT (right) sources. We also included sources presented in WAT-CAT catalogue [Missaglia et al. \(2019\)](#).

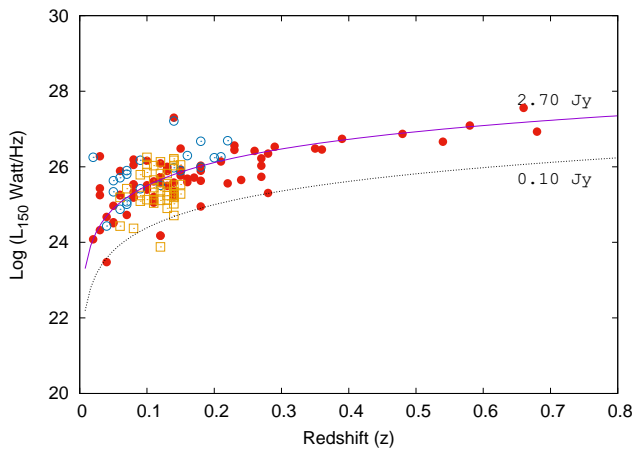


Figure 5. Plot of radio luminosity against redshift for the 103 tailed sources presented in the current paper. The WAT and NAT sources are indicated by red circles and open blue circles, respectively. The yellow squares present wide-angle tailed radio galaxies in the WATCAT catalogue ([Missaglia et al. 2019](#)). The pink solid line indicates the best-fitted luminosity using points from all surveys in the figure, which corresponds to 2.70 Jy flux density for tailed radio sources.

1999). There is a tendency for the majority of powerful radio sources to have higher spectral index. At a low frequency, the spectral index gives us information on the energy index of the synchrotron particles that are injected into the lobes ([Blundell et al. 1999](#)). With the help of enhanced magnetic field, radio sources create high jet kinetic power ([Blundell et al. 1999](#)), which helps fast synchrotron cooling of relativistic electrons. The cooling time (τ) varies with the magnetic field ($\tau \propto \frac{1}{B^2}$). At last, the magnetic field enhances

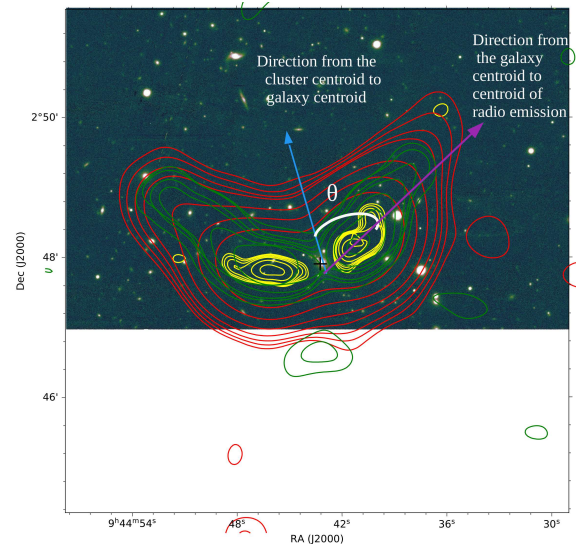


Figure 6. A figure showing an example of a measurement of the bending angle of a tailed radio source. PanSTARRS r-band optical images are overlaid with TGSS (green contour), NVSS (red contour), and FIRST (yellow contour) images. The '+' symbol is the position of the host galaxy from PanSTARRS r-band where two radio tails are terminated. The blue arrow indicates the direction from the cluster centroid to the galaxy centroid, and the magenta arrow shows the direction from the galaxy centroid to the centroid of the radio emission peak in the intensity map. We calculate the angle θ between two arrows. Then 2θ is the bending angle between two radio tails.

the synchrotron loss and make the steeper energy distribution at high radio luminosity.

Figure 5 represents the distribution of tailed radio sources in the log $L-z$ plane. Most of the sources are within the redshift range of 0.1 to 0.4, and the number of radio sources decreases with increasing redshift beyond $z = 0.5$. There are no available sources in the lower right quadrant of Figure 5

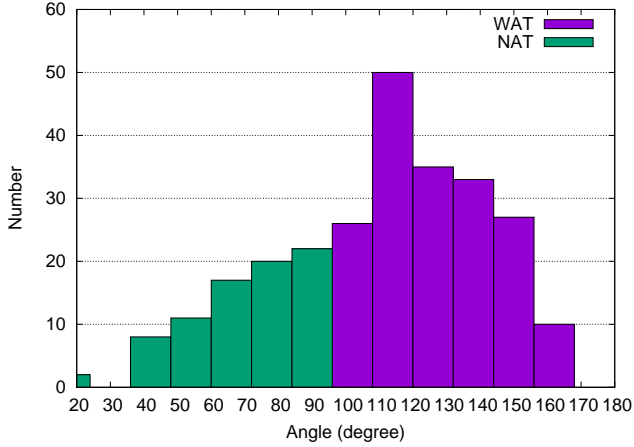


Figure 7. Distribution showing source count vs bending angle of the tailed galaxies. The green and blue bars indicate the number of NAT and WAT sources respectively in the range of a particular bending angle.

which is due to the non-identification of low luminosity radio galaxies at high redshift. This sensitivity limit of the survey is known as the Malmquist bias (Malmquist 1922, 1936). The Malmquist bias means that there will be a tight correlation between luminosity and redshift in a single flux-limited sample. A tight correlation depends on (i) the steepness of the distribution in jet kinetic powers, (ii) the energy distribution of the particles injected into lobes (Blundell et al. 1999). This is expected because radio luminosity strongly correlates with the above two parameters. But, at high redshift, a negative correlation is established between projected linear size and redshift.

Based on the availability of redshift data, we estimate L_{150} for 79 WATs and 21 NATs from our catalogue. The mean and median L_{150} of WATs and NATs confirm that WATs and NATs have the same distribution of the radio luminosity which implies that governing conditions in the core engines of WATs and NATs may be same. The mean and median of $\log L$ [W Hz^{-1}] of WATs in Missaglia et al. (2019) are 25.40 and 25.35, and in Pal & Kumari (2021) are 25.59 and 25.60 respectively, which indicate that our tailed radio galaxies are similar luminous compared to tailed radio galaxies in the FIRST and LOFAR catalogues.

The spectral index features of the tailed radio source population can be used to identify a variety of source characteristics. For example, the radio spectral index is commonly utilised to differentiate between the source components of AGN. The nature of core radio spectral indices is normally flat or inverted. Inverted radiation spectra probably originate in partially optically thick regimes where low frequency radiation is preferentially put down via free-free absorption or synchrotron self-absorption. On the other hand, flat spectra likely arise from the superposition of naturally distinct regions along the jet with dynamically lower frequency turnover. Steep energy spectrum usually comes from lobe components and ultra steep energy spectrum arise for the relic emission (Mahony et al. 2016). All previous

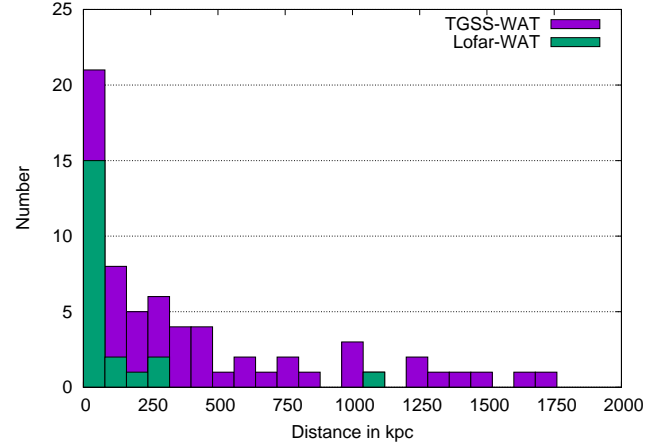


Figure 8. Distribution of distance of tailed radio galaxies from the galaxy cluster centre. We also included sources presented in LoFAR WATs (Pal & Kumari 2021).

studies (Mahony et al. 2016; Ishwara-Chandra et al. 2010; Kapahi et al. 1998) found the mean spectral index of radio galaxies in the range of 0.7–0.8 and 0.75 are usually considered to be the typical spectral index for radio galaxies (RGs). For example, Mahony et al. (2016) found radio galaxies with spectral index in the range -0.5 to 1.5 with median= 0.78 and Ishwara-Chandra et al. (2010) found radio galaxies with spectral index in the range -0.5 to 2.5 with median= 0.78 . The mean and median of the spectral index of tailed radio sources presented in the current article is close to the spectral index of a typical radio galaxy which implies that tailed radio galaxies and normal radio galaxies are similar in terms of the properties of their spectral index.

Figure 8 shows the distribution of distance of WATs with respect to the centre of host cluster. The cluster centric distance distribution peak is seen at distance < 250 kpc. For distances above ~ 600 kpc the fraction of WATs drops quickly. This figure shows that the majority of the WATs are lying close to the cluster center and the number of WATs decreases with the distance from the centre of a galaxy cluster. WATs usually settle in the cluster centre, i.e., at the bottom of the potential well (Gunn et al. 2006). The relative velocities of WATs with respect to the background are thought to be low (Leahy & Williams 1984). It is also known that the merger between two clusters could induce shocks which passage through the radio galaxies and could also affect the wide jet morphology (Gan et al. 2017). NATs are usually field galaxies moving through their host cluster with high velocity $\sim 2500 \text{ km s}^{-1}$ (e.g., NGC 1265 Sun et al. (2005)). NATs and WATs originate from the same physical processes, but jet physics are different as a result of the different environments.

5.2 Cluster mass and tailed radio galaxies

The bending of jets is affected by the mass of the parent cluster in two ways. Firstly, the cluster mass is correlated with the density of the inter-cluster medium for which heavier clusters experience the denser inter-cluster medium.

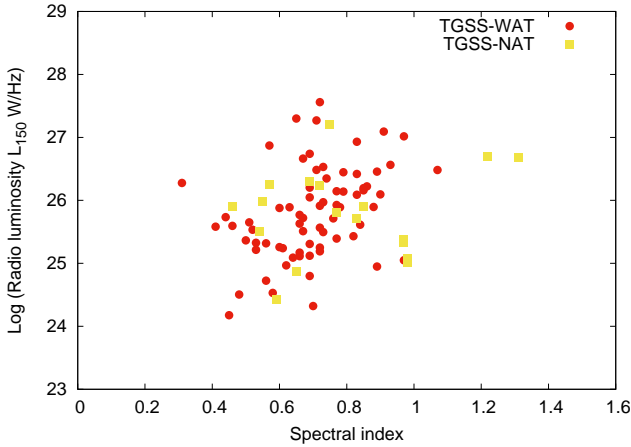


Figure 9. Plot shows spectral index variation with radio luminosity of tailed radio galaxies.

Secondly, the mass of the cluster is correlated with the velocity dispersion of galaxies, which results in faster movement of galaxies in high mass clusters (Mguda et al. 2015). According to a simulation by Mguda et al. (2015), there are no tailed radio galaxies in clusters with masses less than $10^{13} M_{\odot}$ and only a few in clusters with masses less than $10^{13.5} M_{\odot}$. Another simulation suggests the presence of over 50000 galaxy clusters in the $10^{13} M_{\odot} - 10^{14} M_{\odot}$ mass range and over 4000 galaxy clusters with masses larger than $10^{14} M_{\odot}$ which give proper favourable conditions for radio jet bending (Gottlöber et al. 2006). The majority of tailed radio galaxies are seen in clusters with the mass range $10^{14} M_{\odot}$ and $10^{15} M_{\odot}$. Clusters above $10^{14.5} M_{\odot}$ are expected to host at least one-tailed galaxy at some point during their lifetime (Mguda et al. 2015). In tables 3 and 4, we summarise different properties of clusters corresponding to WAT and NAT galaxies detected in the current paper. The mass and radius are two important properties of a cluster. The widely used parameters of a cluster are r_{500} , the radius within which the mean density of a cluster is 500 times of the critical density of the Universe ($\rho_c = \frac{3H^2(z)}{8\pi G}$), and M_{500} , the cluster mass within r_{500} . We calculate the cluster optical mass M_{500} (in unit of $10^{14} M_{\odot}$) from cluster richness (R_L) which is closely correlated as (Wen et al. 2015)

$$\log M_{500} = (1.08 \pm 0.02) \log R_L - (1.37 \pm 0.02), \quad (10)$$

We find host clusters for 118 tailed sources using 22 known cluster catalogues summary of which is shown in Table 5. The maximum clusters can be also found from the WHL cluster catalogue which provides optical richness and optical mass (M_{500}). The range of optical mass (M_{500}) of clusters lies in between $0.27 \times 10^{14} M_{\odot} - 13.06 \times 10^{14} M_{\odot}$. Four of these clusters come from X-ray cluster catalogues. We calculate the corresponding optical masses of galaxy clusters from MCXC cluster catalogue using their optical properties from Wen et al. (2012); Wen et al. (2015). We find that the majority (166 of 284 total) of tailed radio galaxies in our sample have no association with known clusters or groups. The detected WAT

and NAT sources should be used to search for nearby clusters. There are 10 clusters found in relatively low-mass clusters (of the order of $10^{14} M_{\odot}$).

6 SUMMARY

We have presented 264 new tailed galaxy candidates from the visual inspection of the 150 MHz TGSS survey out of which 203 are WAT type and 61 are NAT type sources. We found 192 sources from the northern sky and 72 sources from the southern sky. Because of the low radio frequency used in the survey, a significant number of steep-spectrum sources are seen. The summary of the paper is as follows:

- We report a sample of 264 tailed radio galaxies. This makes it the largest sample of tailed radio galaxies discovered to date. Out of 264 new tailed galaxies, 203 are WAT type galaxies and 61 are NAT type galaxies.
- We report a sample of 264 tailed radio galaxies. This makes it the largest sample of tailed radio galaxies discovered to date. Out of 264 new tailed galaxies, 203 are WAT type galaxies and 61 are NAT type galaxies.
- The optical/IR counterparts of 261 sources are found, and redshift is available for 112 sources. About 45 per cent (92/203) WATs and 32 per cent (20/61) NATs are identified by redshift.
- The total integrated flux density of sources in our sample at 150 MHz ranges from 0.1 Jy to as large as 20.1 Jy.
- In our sample of tailed radio galaxies, two-tailed galaxies (WAT-J0932+5533 and NAT-J2038-2011) is hosted by quasars.
- The high-resolution deep radio observations of TGSS-ADR images have enabled us to find tailed radio galaxies with less luminosity at 150 MHz. J0856+4829 is the least luminous WAT in our sample with $L_{150} = 1.5 \times 10^{24} \text{ W Hz}^{-1}$ ($z = 0.12$) and J0549-2520 is the least luminous NAT in our sample with $L_{150} = 2.7 \times 10^{24} \text{ W Hz}^{-1}$ ($z = 0.04$). J0225+4031 is the most luminous WAT in our sample with $L_{150} = 1.9 \times 10^{27} \text{ W Hz}^{-1}$ ($z \sim 0.65$) and J1314+6220 is the most luminous NAT in our sample with $L_{150} = 162.8 \times 10^{25} \text{ W Hz}^{-1}$ ($z = 0.14$).
- The spectral index peaks near 0.75 for both WATs and NATs. For WAT, the total span of α_{150}^{1400} is from 0.02 to 1.70 and for NATs, the total span of α_{150}^{1400} is from 0.38 to 2.04.
- The measured span of optical mass of host galaxy clusters for M_{500} is $12.33 \times 10^{14} M_{\odot} - 0.52 \times 10^{14} M_{\odot}$.
- The range of the calculated density of galaxy clusters is from $206.7 \text{ (Mpc}^{-3})$ to $36.3 \text{ (Mpc}^{-3})$.

ACKNOWLEDGEMENTS

We thank the whole TGSS team and the staff of the GMRT behind this survey. GMRT is run by the National Centre for Radio Astrophysics of the Tata Institute of Fundamental Research. This research has made use of the ‘‘Aladin sky atlas’’ developed at CDS, Strasbourg Observatory, France and the NASA/IPAC Extragalactic Database (NED) operated by the Jet Propulsion Laboratory, California Institute of Technology. This publication makes use of data products from the Two Micron All Sky Survey, which is a joint project of the University of Massachusetts and the Infrared Processing and

Analysis Center/California Institute of Technology, funded by the National Aeronautics and Space Administration and the National Science Foundation.

DATA AVAILABILITY STATEMENT

The data that support the plots within this paper and other findings of this study are available from the corresponding author upon reasonable request. The TGSS ADR 1 images are available at <http://tgssadr.strw.leidenuniv.nl/doku.php>.

REFERENCES

- Abell G. O., 1958, *ApJS*, 3, 211
- Abell G. O., Corwin H. G. Jr., Olowin R. P., 1989, *ApJS*, 70, 1
- Adams M., Jensen E., and Stocke J. 1980, *AJ*, 85,1010
- Aghanim et al., 2020, *A&A*, 641, 67
- Alam S. et al., 2015, *ApJS*, 219, 12
- Allen S. W., Evrard A. E., and Mantz A. B., 2011, *ARA&A*, 49, 409
- Baan W. A., McKee M. R., 1985, *A&A*, 143, 136
- Baan W. A. and McKee M. R. 1985, *A&A*, 143, 136
- Bliton M., Rizza E., Burns J. O., Owen F. N., & Ledlow, M. J. 1998, *MNRAS*, 301, 609
- Begelman M. C., Rees M. J., Blandford R. D., 1979, *Nature*, 279, 770
- Becker R. H., White R. L., Helfand D. J., 1995, *ApJ*, 450, 559
- Bennett C. L., Lawrence C. R., Burke B. F., Hewitt J. N., Mahoney J., 1986, *ApJS*, 61, 1
- Belsole E., Worrall D. M., Hardcastle M. J. and Croston J. H., 2007, *MNRAS*, 381, 1109
- Berlind A. A., Frieman J., Weinberg D., et al., 2006, *ApJS*, 167, 1
- Blanton E. L., Gregg M. D., Helfand D. J., Becker R. H., White R. L., 2000, *ApJ*, 531, 118
- Bhukta N, Pal S., Mondal S., 2020, *MNRAS*, submitted, astro-ph:2006.07219
- Bhukta N., Mondal S. K., Pal S., 2021, in prep.
- Blanton E. L., Gregg M. D., Helfand D. J., Becker R. H., Leighly K. M., 2001, *AJ*, 121, 2915
- Blanton E. L., Gregg M. D., Helfand D. J., Becker R. H., White R. L., 2003, *AJ*, 125, 1635
- Bleem L. E. et al., 2015, *ApJs*, 216, 27
- Blundell K. M., Rawlings S. and Willott C. J., 1999, *AJ*, 117, 677
- Bolton J., Gardner F., Mackey M., 1964, *Australian J. Phys.*, 17, 340
- Bonzini M., Mainieri V., Padovani V., et al. 2012, *ApJs*, 203, 15
- Bolton J. G., Clarke M. E., Ekers R. D., 1965, *Aus. J. Phy.*, 18, 627
- Bridle A. H., Fomalont E. B., Palimaka J. J., and Willis A. G., 1981, *ApJ*, 248, 499
- Burns J. O., 1981, *MNRAS*, 195, 523
- Burns J. O., Balonek T. J., 1982, *ApJ*, 263, 546
- Burns J. O., Eilek J. A., & Owen F. N. 1982, in *IAU Symp. 97, Extragalactic Radio Sources*, ed. D. Heeschen & C. Wade (Dordrecht: Reidel), 45
- Burns J. O., O’Dea C. P., Gregory S. A., Balonek T. J., 1986, *ApJ*, 307, 73
- Caswell J. L., Crowther J. H., 1969, *MNRAS*, 145, 181
- Chambers K. C., Magnier E. A., Metcalfe N., et al. 2016, *ArXiv e-prints* [arXiv:1612.05560]
- Chincarini G., Rood H. J., 1976, *Publications of the Astronomical Society of the Pacific (PASA)*, 88, 388
- Chon G., Bohringer H., Nowak N., 2013, *MNRAS*, 429, 3272
- Cohen A. S., Lane W. M., Cotton W. D., Kassim N. E., Lazio T. J. W., Perley R. A., Condon J. J., Erickson W. C., 2007, *AJ*, 134, 1245
- Ciliegi P., Zamorani G., Hasinger G., et al. 2003, *A&A*, 398, 901
- Colla G. et al., 1970, *A&AS*, 1, 281
- Colla G. et al., 1972, *A&AS*, 7, 1
- Colla G. et al., 1973, *A&AS*, 11, 291
- Condon J. J., Cotton W. D., Greisen E. W., Yin Q. F., Perley R. A., Taylor G. B., Broderick J. J., 1998, *AJ*, 115, 1693
- Cowie L. L. & McKee C. F., 1975, *A&A*, 43, 337
- Cutri R. M., Strutskie M. F., van Dyk S., et al. 2013, *VizieR Online Data Catalog: II/328*
- Dalton G. B., Maddox S. J., Sutherland W. J., Efstathiou G., 1997, *MNRAS*, 289, 263
- Dehghan S., Johnston-Hollitt M., Franzen T. M. O., Norris R. P., and Miller N. A., 2014, *Aj*, 148, 5
- de Ruiter H. R., Willis A. G., and Arp H. C. 1977, *A&A*, 28, 211
- Donoso E., Best P. N., Kauffmann G., 2009, *MNRAS*, 392, 617
- Douglass E. M., Blanton E. L., Clarke T. E., Randall S. W., Wing J. D., 2011, *ApJ*, 743, 193
- Ebeling Harald., Mullis Christopher R., Tully R. Brent., 2002, *ApJ*, 580, 74
- Eke V. R., 2004, *MNRAS*, 348, 866
- Eilek J. A., Burns J. O., O’Dea C. P., & Owen, F. N., 1984, *ApJ*, 278, 37
- Eilek J. A., and Owen F. N. 2002, *ApJ*, 567, 202
- Eke et al., 2004, *MNRAS*, 348, 866
- Feretti L., Giovannini G., Klein U., et al., 1998, *A &A*, 331, 475
- Fanaroff B. L., Riley J. M., 1974, *MNRAS*, 167, 31
- Ficarra A., Grueff G., Tomassetti G., 1985, *A&A*, 59, 255
- Feretti L., Dallacasa D., Govoni F., Giovannini G., Taylor G. B., Klein U., 1999, *A&A*, 344, 472
- Gunn J, E. et al., 2006, *AJ*, 131, 2332
- Gan Z., Li H., Li S. and Yuan F., 2017, *APJ*, 839, 14
- Gal R. R., Lopes P. A. A., de Carvalho R. R., Kohl-Moreira J. L., Capelato H. V., Djorgovski S. G., 2009, *AJ*, 137, 298
- Giacintucci S., Venturi A, 2009, *A&A*, 505, 5561
- Goto Tomotsugu. et al., 2002, *AJ*, 123 1807
- Gottlöber S., Yepes G., Khalatyan A., Sevilla R., Turchaninov V., 2006, in Manoz C., Yepes G., eds, *The Dark Side of the Universe Vol. 878 of American Institute of Physics Conference Series*, Dark and baryonic matter in the MareNostrum Universe. pp 3
- Gower J. F. R., Scott P. F., Wills D., 1967, *MNRAS*, 71, 49
- Gregory P. C., Condon J. J., 1991, *ApJS*, 75, 1011
- Gruppioni C., Zamorani G., de Ruiter H. R., et al. 1997, *MNRAS*, 286, 470
- Griffith M. R., Wright A. E., Burke B. F., Ekers R. D., 1994, *ApJS*, 90, 179
- Hales S. E. G., Baldwin J. E., Warner P. J., 1988, *MNRAS*, 234, 919
- Hales S. E. G., Masson C. R., Warner P. J., Baldwin J. E., 1990, *MNRAS*, 246, 256
- Hales S. E. G., Mayer C. J., Warner P. J., Baldwin J. E., 1991, *MNRAS*, 251, 46
- Hales S. E. G., Baldwin J. E., Warner P. J., 1993a, *MNRAS*, 263, 25
- Hales S. E. G., Masson C. R., Warner P. J., Baldwin J. E., Green D. A., 1993b, *MNRAS*, 262, 1057
- Hardcastle M. J., Worrall D. M., Kraft R. P., Forman W. R., Jones C., and Murray S. S., 2003, *ApJ*, 593, 169
- Hardcastle M. J., Sakelliou I., and Worrall D. M. 2005, *MNRAS*, 359, 1007
- Hao Jiangang, et al., 2010, *ApJS*, 191, 254
- Healey Stephen E., et al., 2007, *ApJS*, 171, 61
- Hill G. J. and Lilly S. J., 1991, *ApJ*, 367, 1
- Huchra J. P., Vogeley M. S., and Geller M. J. 1999, *ApJS*, 121, 287

Table 1. Candidate WAT radio sources

Cat NO.	Name	R.A-core (J2000.0)	Dec-core (J2000.0)	Separation (arsec)	ρ	F_{150} (Jy)	F_{1400} (Jy)	$\alpha_{0.15}^{1.4}$ (± 0.05)	z	L_{150} WHz^{-1} $\times 10^{25}$	Other Catalog
(1)	(2)	(3)	(4)	(5)	(6)	(7)	(8)	(9)	(10)	(11)	(12)
1	J0001+5458	00 01 21.8	+54 58 10	5.20	0.90	0.59	0.10	0.79	–	–	1, 8
2	J0003–3556	00 03 11.5	–35 56 38	2.12	0.99	7.16	–	–	0.05	–	14
3	J0005+5359	00 05 46.3	+53 59 57	3.50	0.99	0.67	0.09	0.89	–	–	1, 8
4	J0008–3347	00 08 49.6	–33 47 51	6.03	0.89	0.33	0.03	1.07	–	–	1, 14
5	J0022+2317	00 22 24.4	+23 17 25	5.14	0.99	2.14	0.41	0.73	0.13	9.36	1
6	J0041+2104	00 41 43.1	+21 04 26	5.01	0.99	0.35	0.33	0.02	–	–	1
7	J0050+0514	00 50 44.6	+05 15 01	3.12	0.99	0.27	0.10	0.44	0.27 ^b	5.42	1
8	J0054+3339	00 54 43.8	+33 39 01	6.58	0.99	0.33	0.06	0.76	–	–	1, 4
9	J0104+8210	01 04 25.1	+82 10 31	6.47	0.89	0.66	0.19	0.55	–	–	1, 4
10	J0106+4909	01 06 48.6	+49 08 56	9.28	0.99	0.43	0.07	0.81	–	–	1
11	J0114+0029	01 14 25.6	+00 29 33	6.69	0.99	0.36	0.09	0.62	0.35	13.46	11
12	J0119+5838	01 19 35.3	+58 38 54	4.71	0.99	0.55	0.08	0.86	–	–	1, 8
13	J0120+1451	01 20 01.1	+14 51 38	6.29	0.88	0.59	0.16	0.58	0.05 ^b	0.34	1, 8
14	J0123+3315	01 23 39.9	+33 15 22	0.29	0.99	1.43	0.10	1.19	0.02	0.12	1
15	J0128+3448	01 28 59.1	+34 48 42	6.18	0.99	0.73	0.14	0.73	0.15	04.32	1,4
16	J0139+7444	01 39 25.2	+74 44 58	2.31	0.99	0.15	0.04	0.59	–	–	1, 8
17	J0141+4506	01 41 37.0	+45 06 07	2.10	0.99	0.31	0.09	0.55	–	–	1
18	J0149+1403	01 49 11.9	+14 03 01	6.22	0.99	0.46	0.13	0.56	0.07	0.53	1
19	J0200+3935	02 00 53.0	+39 35 01	6.46	0.99	1.80	0.61	0.48	–	–	10
20	J0203+6702	02 03 08.5	+67 02 52	1.95	0.99	0.89	0.12	0.89	–	–	1, 4
21	J0204+0415	02 04 28.9	+04 15 17	4.95	0.99	0.33	0.10	0.53	0.14 ^a	1.64	11
22	J0205–4124	02 05 40.4	–41 24 13	6.08	0.99	1.10	–	–	–	–	–
23	J0209+0950	02 09 47.6	+09 50 02	3.68	0.96	4.69	1.25	0.59	–	–	1
24	J0225+4031	02 25 44.9	+40 31 33	1.49	0.95	3.93	0.91	0.65	0.14	199.09	3
25	J0228+3821	02 28 30.3	+38 21 12	7.77	0.99	1.07	0.22	0.70	0.03	0.21	4, 10
26	J0229+3942	02 29 47.8	+39 42 29	1.34	0.99	0.98	0.15	0.84	–	–	4, 10
27	J0245+8207	02 45 20.2	+82 07 15	1.61	0.99	1.38	0.18	0.91	–	–	1
28	J0257–0400	02 57 43.8	–03 59 59	3.61	0.99	1.10	–	–	0.18 ^b	–	6, 11
29	J0300+7438	03 00 32.1	+74 38 59	–	–	2.36	0.32	0.89	–	–	1, 2
30	J0303+3856	03 03 0.44	+38 56 39	9.98	0.98	0.95	0.18	0.74	0.28 ^a	22.28	1,4
31	J0306–1206	03 06 58.6	–12 06 43	3.31	0.99	5.94	1.39	0.65	–	–	1, 2
32	J0310+4803	03 10 16.9	+48 03 27	2.17	0.99	2.07	0.55	0.59	–	–	1, 3
33	J0312+0644	03 12 51.7	+06 44 48	7.42	0.99	0.41	0.06	0.86	–	–	1
34	J0315+0507	03 15 30.6	+05 07 46	5.30	0.99	0.38	0.10	0.59	–	–	1
35	J0316+0922	03 15 59.9	+09 23 01	3.89	0.82	0.45	0.13	0.55	–	–	6
36	J0317+4917	03 17 33.3	+49 17 19	4.43	0.89	1.56	0.40	0.60	–	–	1, 8
37	J0338+1544	03 38 04.5	+15 44 19	11.7	0.93	0.16	0.08	0.31	0.03 ^b	18.92	1
38	J0348+1924	03 48 28.4	+19 24 19	10.1	0.98	1.23	0.23	0.75	–	–	1
39	J0401+3853	04 01 4.30	+38 53 00	4.15	0.65	0.55	0.13	0.64	–	–	1, 10
40	J0402+1929	04 02 13.0	+19 29 07	8.54	0.64	2.58	0.78	0.53	–	–	1
41	J0405–2610	04 05 15.9	–26 10 58	1.23	0.99	0.93	0.18	0.73	–	–	1
42	J0415+3428	04 15 13.5	+34 28 29	3.23	0.99	0.68	0.14	0.70	–	–	1, 4, 8
43	J0436+0603	04 36 22.5	+06 03 12	7.63	0.99	1.45	0.24	0.70	–	–	1
44	J0458+8206	04 58 38.3	+82 06 35	4.50	0.99	0.51	0.08	0.82	–	–	2, 4
45	J0505+1056	05 05 08.1	+10 56 08	2.11	0.99	1.34	0.28	0.70	–	–	1
46	J0508+2754	05 08 12.3	+27 54 15	4.64	0.87	2.36	0.40	0.79	–	–	1
47	J0520+1356	05 20 12.5	+13 56 01	4.77	0.99	0.95	0.22	0.65	–	–	1, 3
48	J0522+2807	05 22 46.0	+28 06 40	6.65	0.99	1.91	–	–	–	–	–
49	J0528+5601	05 28 38.3	+56 01 49	1.33	0.99	0.43	0.07	0.81	–	–	4
50	J0533+4727	05 33 54.8	+47 27 07	10.5	0.82	2.49	0.34	1.12	–	–	1, 4, 10
51	J0542+7902	05 42 58.0	+79 02 31	–	–	0.61	0.16	0.59	–	–	15
52	J0602+1937	06 02 37.2	+19 37 05	4.57	0.99	0.85	0.14	0.80	–	–	1, 8
53	J0602+2911	06 02 34.1	+29 11 06	9.66	0.82	2.99	0.48	0.81	–	–	1, 2
54	J0608+8058	06 08 32.1	+80 58 12	1.52	0.99	0.77	0.16	0.70	–	–	1, 4
55	J0623+0504	06 23 11.5	+05 04 12	4.29	0.99	0.85	0.15	0.77	–	–	1, 6
56	J0626+2838	06 26 38.6	+28 38 42	2.16	0.99	0.72	0.09	0.93	–	–	1, 8, 9
57	J0630+2306	06 30 31.4	+23 06 05	6.02	0.99	0.52	0.09	0.78	–	–	16
58	J0631+2500	06 31 25.8	+25 00 48	1.94	0.99	13.3	1.08	1.12	0.08 ^a	3.39	1
59	J0640+1020	06 40 41.6	+10 20 36	6.20	0.95	0.56	0.12	0.68	–	–	1,15
60	J0645+1340	06 45 28.0	+13 40 25	–	–	1.01	0.13	0.91	–	–	1, 2

Table 1 – *continued* Candidate WAT radio sources

Cat NO.	Name	R.A-core (J2000.0)	Dec-core (J2000.0)	Separation (arsec)	ρ	F_{150} (Jy)	F_{1400} (Jy)	$\alpha_{0.15}^{1.4}$ (± 0.05)	z	L_{150} WHz^{-1} $\times 10^{25}$	Other Catalog
(1)	(2)	(3)	(4)	(5)	(6)	(7)	(8)	(9)	(10)	(11)	(12)
61	J0653+6919	06 53 17.8	+69 19 39	4.41	0.99	8.18	1.38	0.79	–	–	1, 2, 4
62	J0655+0412	06 55 20.3	+04 12 09	3.14	0.99	2.49	0.30	0.94	–	–	6
63	J0700+2736	07 00 01.0	+27 36 28	5.94	0.99	1.73	0.31	0.76	–	–	1,9
64	J0708+2928	07 08 48.5	+29 28 13	5.24	0.99	1.22	0.16	0.90	0.19	12.44	1,9
65	J0714+1334	07 14 10.5	+13 34 49	6.33	0.99	0.45	0.10	0.67	0.54	46.12	1, 8
66	J0715–3044	07 15 24.8	–30 43 45	10.1	0.96	1.65	0.30	0.76	–	–	1
67	J0724+5010	07 24 31.5	+50 10 53	3.96	0.61	1.00	0.15	0.84	–	–	1, 8, 11
68	J0736+2412	07 36 21.8	+24 12 14	5.29	0.99	4.88	0.44	1.07	0.15	30.35	1, 2
69	J0752+0814	07 52 57.0	+08 14 33	7.20	0.93	0.64	0.04	1.24	–	–	1, 2
70	J0756+0107	07 56 7.31	+01 07 48	4.37	0.76	1.30	0.41	0.51	–	–	1
71	J0757+3640	07 57 53.2	+36 40 22	6.91	0.99	1.44	0.32	0.67	0.12 ^a	5.25	12, 13
72	J0805+1614	08 05 44.8	+16 14 05	2.46	0.99	1.01	0.18	0.77	0.10 ^b	2.48	12
73	J0818+5437	08 18 06.6	+54 37 32	3.18	0.99	3.31	0.51	0.83	0.12 ^b	12.28	11
74	J0831+6104	08 31 48.8	+61 04 59	9.36	0.98	1.24	0.14	0.97	–	–	1
75	J0841+4451	08 41 04.3	+44 51 04	1.86	0.65	0.48	0.07	0.86	0.27	10.67	1, 10, 11
76	J0856+4829	08 56 1.17	+48 29 20	10.2	0.99	0.44	0.16	0.45	0.12 ^b	0.15	4, 8, 11
77	J0912+1600	09 12 35.2	+16 00 01	7.33	0.99	0.10	0.02	0.72	0.08 ^b	1.55	1
78	J0917+5509	09 17 08.0	+55 09 08	4.34	0.99	1.30	0.22	0.79	0.19	13.13	4,8
79	J0932+5533	09 32 01.0	+55 33 47	0.80	0.99	0.81	0.17	0.69	0.26 ^b	15.92	1, 11
80	J0940+1131	09 40 34.4	+11 31 40	3.94	0.99	2.76	0.58	0.69	0.08 ^b	1.32	1
81	J0944+0247	09 44 43.4	+02 47 57	2.96	0.68	3.73	0.35	1.05	0.22	03.64	1,6
82	J0951–0757	09 51 30.2	–07 57 51	3.81	0.99	0.72	–	–	–	–	–
83	J0957–0644	09 57 00.4	–06 44 26	8.44	0.99	2.27	0.40	0.77	0.13	9.96	1,6
84	J1003+1019	10 03 41.9	+10 20 01	5.33	0.99	0.69	0.20	0.55	0.18	0.89	1, 11, 16
85	J1008–4055	10 08 11.0	–40 55 44	9.12	0.99	0.66	–	–	–	–	14
86	J1009–1504	10 09 07.3	–15 04 04	1.67	0.92	1.96	0.12	1.25	–	–	1, 2
87	J1012+0841	10 12 06.4	+08 41 33	5.88	0.99	0.87	0.21	0.63	0.09	01.72	1,11
88	J1015+1221	10 15 41.1	+12 21 01	7.41	0.99	0.35	0.10	0.56	–	–	1, 11
89	J1019+7020	10 19 56.1	+70 20 22	5.42	0.99	0.72	0.12	0.80	–	–	1, 4, 8
90	J1022+5006	10 22 28.4	+50 06 20	4.24	0.65	0.73	0.03	1.42	0.16	05.51	2,4
91	J1032+3151	10 32 18.0	+31 51 42	3.60	0.99	0.79	0.16	0.71	0.35	30.40	1, 9, 11
92	J1034+0736	10 34 10.0	+07 36 05	3.76	0.97	0.92	0.12	0.91	0.58 ^b	123.92	1, 2, 11
93	J1038–3346	10 38 47.9	–33 46 35	3.97	0.99	0.50	0.06	0.94	–	–	1
94	J1042+0237	10 42 31.3	+02 37 10	8.65	0.99	0.87	0.12	0.88	0.18 ^b	7.85	1, 6, 11
95	J1046–2911	10 46 09.9	–29 21 10	3.48	0.99	2.14	0.55	0.60	0.06	1.81	1
96	J1048+3532	10 48 49.0	+35 32 01	3.51	0.99	1.94	0.22	0.97	0.39	104.11	1, 4, 13
97	J1050+0432	10 50 57.6	+04 32 17	10.2	0.99	0.34	0.08	0.64	0.12	1.23	1
98	J1050–2405	10 50 34.5	–24 05 57	5.95	0.99	3.19	0.67	0.69	0.03	0.63	1
99	J1051+1825	10 51 57.7	+18 25 38	5.61	0.99	0.49	0.11	0.66	0.55 ^b	1.48	1, 11
100	J1056+0255	10 56 17.0	+02 55 26	1.94	0.97	0.54	0.07	0.91	0.39	28.40	1
101	J1058+0136	10 58 07.5	+01 36 19	2.34	0.99	1.26	0.04	1.54	0.04	0.47	1, 2
102	J1106–4018	11 06 58.0	–40 18 55	10.5	0.93	0.65	–	–	–	–	14
103	J1108–4424	11 08 11.0	–44 24 30	1.68	0.62	0.55	–	–	–	–	14
104	J1108+2610	11 08 12.5	+26 10 34	5.96	0.95	0.66	0.12	0.76	0.17 ^b	5.16	11, 13
105	J1116–3010	11 16 00.1	–30 10 08	1.95	0.99	0.73	0.12	0.80	–	–	1
106	J1118+2754	11 18 59.4	+27 54 07	7.10	0.99	2.05	0.52	0.61	0.06	1.74	11
107	J1119+6317	11 19 33.2	+63 17 17	4.39	0.99	0.42	0.11	0.59	0.16	02.80	1,4,11
108	J1120+2912	11 20 38.5	+29 12 34	5.26	0.99	0.28	0.08	0.56	0.24 ^b	4.48	1, 11
109	J1130+2524	11 30 48.8	+25 24 36	2.99	0.99	0.41	0.09	0.67	0.14 ^b	2.08	1, 11
110	J1131+4408	11 31 10.1	+44 08 15	10.1	0.85	0.49	0.06	0.94	–	–	1, 2, 10
111	J1132+6311	11 32 51.0	+63 11 44	3.59	0.99	1.90	0.43	0.66	0.11 ^b	1.30	1, 4
112	J1141–3357	11 41 28.9	–35 57 10	5.45	0.99	0.32	–	–	–	–	1
113	J1142+1102	11 42 54.3	+11 01 33	8.53	0.99	1.30	0.34	0.60	0.15 ^b	7.57	17
114	J1151+0422	11 51 46.9	+04 22 23	2.73	0.86	0.39	0.09	0.65	0.13	01.68	1,11
115	J1155+5755	11 55 58.3	+57 55 27	9.30	0.93	0.38	0.11	0.55	–	–	2, 11
116	J1156+3432	11 56 7.40	+34 32 47	5.32	0.98	1.03	0.15	0.86	–	–	1, 11, 13
117	J1158+2117	11 58 37.2	+21 17 11	5.98	0.99	0.36	0.07	0.73	–	–	1,11

Table 1 – *continued* Candidate WAT radio sources

Cat NO.	Name	R.A-core (J2000.0)	Dec-core (J2000.0)	Separation (arsec)	ρ	F_{150} (Jy)	F_{1400} (Jy)	$\alpha_{0.15}^{1.4}$ (± 0.05)	z	L_{150} WHz^{-1} $\times 10^{25}$	Other Catalog
(1)	(2)	(3)	(4)	(5)	(6)	(7)	(8)	(9)	(10)	(11)	(12)
118	J1200+2942	12 00 46.1	+29 42 58	7.52	0.99	1.20	0.24	0.72	0.16	8.18	11, 13
119	J1202+5802	12 02 3.80	+58 02 08	3.59	0.99	5.70	0.85	0.85	0.10 ^b	14.42	1, 11
120	J1205+3204	12 05 14.5	+32 04 17	5.03	0.99	0.72	0.18	0.62	0.16	04.83	11,13
121	J1206+3152	12 06 47.6	+31 52 31	1.59	0.89	0.80	0.17	0.69	0.25	14.48	11,13
122	J1212-4545	12 12 20.7	-45 45 20	1.99	0.99	1.96	–	–	0.16	–	6
123	J1221-4046	12 21 24.4	-40 46 15	0.96	0.98	0.32	–	–	–	–	14
124	J1234-1045	12 34 29.6	-10 45 25	7.78	0.95	0.34	0.06	0.77	–	–	1
125	J1242-3613	12 42 01.0	-36 13 40	2.28	0.68	1.52	0.28	0.75	–	–	1
126	J1242+5021	12 42 7.40	+50 21 47	1.50	0.99	0.34	0.10	0.54	0.15	01.96	1,8
127	J1249+0144	12 49 42.9	+01 44 18	3.79	0.94	0.50	0.20	0.41	–	–	1
128	J1304+1041	13 04 17.9	+10 40 35	2.53	0.99	0.44	0.05	0.97	0.11 ^b	1.12	1
129	J1304+6439	13 04 28.8	+64 39 38	4.48	0.88	1.83	0.31	0.79	0.23 ^b	27.98	1, 4, 8
130	J1307+5651	13 07 43.7	+56 51 03	2.23	0.99	0.72	0.13	0.76	0.24	08.78	4,8,11
131	J1311-0120	13 11 31.7	-01 20 00	4.88	0.99	1.09	0.05	1.37	0.18	10.68	1
132	J1315+4841	13 15 30.5	+48 41 14	7.67	0.86	0.45	0.07	0.83	0.68 ^b	85.27	1
133	J1325+5736	13 25 11.2	+57 36 01	3.98	0.99	1.63	0.10	1.24	0.12 ^b	5.24	1
134	J1331-0544	13 31 24.3	-05 44 36	4.05	0.99	2.92	0.67	0.66	0.15	5.88	1
135	J1412+7420	14 12 25.8	+74 20 19	1.40	0.99	1.23	0.21	0.79	0.21	13.80	1
136	J1414+0143	14 14 32.6	+01 43 54	6.12	0.99	0.56	0.19	0.48	0.05 ^b	0.32	1
137	J1416+0219	14 16 13.4	+02 19 08	6.46	0.99	0.70	0.25	0.46	0.16 ^b	3.94	1
138	J1440+0328	14 40 39.0	+03 28 37	3.94	0.99	0.61	–	–	0.03	–	2
139	J1449+3959	14 49 0.86	+40 00 44	2.09	0.99	1.68	0.26	0.83	–	–	1, 11, 13
140	J1450+4418	14 50 39.8	+44 18 29	3.10	0.99	1.45	0.28	0.73	0.29 ^b	33.94	1, 13
141	J1501+0752	15 01 57.4	+07 52 27	10.2	0.97	2.55	0.50	0.72	0.66 ^b	362.4	1, 11
142	J1508+3554	15 08 34.1	+35 54 28	9.36	0.68	0.90	0.18	0.72	0.12 ^b	3.68	4, 9
143	J1509+3327	15 09 59.7	+33 27 46	9.84	0.99	0.85	0.17	0.72	0.12 ^b	3.12	1, 13
144	J1543-4345	15 43 13.5	-43 45 01	5.55	0.99	3.39	–	–	–	–	–
145	J1553+1530	15 53 45.5	+15 30 14	3.00	0.98	0.72	0.14	0.73	0.13 ^b	3.14	1, 8, 11
146	J1604+2355	16 04 56.7	+23 55 58	3.13	0.99	4.13	0.66	0.82	0.03	2.70	1, 13
147	J1612+2929	16 12 35.4	+29 29 05	3.85	0.99	0.55	0.11	0.72	0.03	1.78	1, 13
148	J1615+4711	16 15 44.1	+47 11 45	9.56	0.99	4.88	0.57	0.96	–	–	1, 4, 11
149	J1616+0926	16 16 53.2	+09 26 36	7.84	0.89	4.88	0.23	1.36	0.20	60.75	1
150	J1620+2521	16 20 35.8	+25 21 04	1.23	0.99	0.62	0.18	0.55	–	–	1, 13
151	J1627-4336	16 27 01.0	-43 36 20	7.82	0.99	2.35	–	–	–	–	6
152	J1631+0115	16 31 30.4	+01 16 14	2.81	0.95	0.43	0.06	0.88	–	–	1
153	J1631+0501	16 31 06.1	+05 01 27	8.74	0.84	1.19	0.17	0.86	–	–	1
154	J1636+2718	16 36 5.20	+27 18 35	4.28	0.99	1.78	0.43	0.63	0.13 ^b	7.76	1, 9, 11
155	J1658+6256	16 58 47.1	+62 56 25	3.79	0.99	1.31	0.29	0.67	0.10 ^b	3.24	1, 4, 8
156	J1701+6413	17 01 32.0	+64 13 38	6.11	0.99	0.37	0.07	0.74	–	–	1, 4, 8
157	J1711+0449	17 11 53.0	+04 49 28	8.22	0.99	1.37	0.16	0.96	–	–	1, 8
158	J1711+1351	17 11 50.9	+13 51 51	5.82	0.99	0.44	0.24	0.27	–	–	1
159	J1717+3734	17 17 25.4	+37 34 59	5.14	0.99	0.37	0.15	0.40	0.09	00.71	1,13
160	J1719+1557	17 19 39.6	+15 57 40	1.08	0.99	3.60	0.08	1.70	–	–	1
161	J1727-2815	17 27 01.1	-28 15 30	1.04	0.99	2.34	0.06	1.64	–	–	1, 15
162	J1729-4330	17 29 56.8	-43 30 55	2.61	0.99	0.76	0.19	0.62	–	–	1, 6
163	J1735+3137	17 35 06.5	+31 37 51	9.00	0.99	0.56	0.12	0.69	0.28	2.03	1, 9
164	J1736+1414	17 36 19.4	+14 14 58	1.59	0.52	0.46	0.07	0.84	–	–	1
165	J1741-3831	17 41 01.0	-38 32 05	3.65	0.99	0.76	0.19	0.62	–	–	1, 6
166	J1741+1720	17 41 39.2	+17 20 34	9.43	0.99	9.05	1.58	0.78	0.06	7.78	1
167	J1748+1400	17 48 26.2	+14 00 54	7.16	0.82	1.14	0.11	1.04	–	–	1, 2
168	J1752+5218	17 52 52.6	+52 17 56	6.35	0.99	0.19	0.03	0.82	–	–	1
169	J1801+2109	18 01 48.5	+21 09 27	7.23	0.86	4.48	0.84	0.75	–	–	1
170	J1814-2302	18 14 39.5	-23 02 38	10.5	0.99	1.73	0.09	1.32	–	–	1
171	J1816+1415	18 16 29.2	+14 15 09	8.54	0.99	3.28	0.60	0.76	–	–	1, 2
172	J1818+1739	18 18 08.5	+17 39 42	10.5	0.98	0.99	0.10	1.02	–	–	1
173	J1820+0855	18 20 2.20	+08 55 14	8.40	0.72	1.87	0.25	0.90	–	–	15, 16
174	J1820+2011	18 20 25.5	+20 11 55	0.53	0.99	0.37	0.07	0.74	–	–	1
175	J1826+3449	18 26 50.2	+34 49 40	2.54	0.93	3.72	0.12	1.53	–	–	1, 9
176	J1827+6832	18 27 31.8	+68 32 15	3.47	0.99	0.76	0.15	0.72	–	–	1, 5
177	J1856+3556	18 56 24.3	+35 56 18	5.96	0.98	1.87	0.57	0.53	–	–	1, 2, 9

Table 1 – continued Candidate WAT radio sources

Cat No.	Name	R.A-core (J2000.0)	Dec-core (J2000.0)	Separation (arcsec)	ρ	F_{150} (Jy)	F_{1400} (Jy)	$\alpha_{0.15}^{1.4}$ (± 0.05)	z	L_{150} WHz^{-1} $\times 10^{25}$	Other Catalog
(1)	(2)	(3)	(4)	(5)	(6)	(7)	(8)	(9)	(10)	(11)	(12)
178	J1906-0033	19 06 16.0	-00 33 29	3.82	0.99	0.92	0.18	0.73	–	–	1, 8
179	J1922+3920	19 22 14.7	+39 20 19	4.76	0.99	2.36	0.58	0.62	–	–	1, 9
180	J1926+4124	19 26 47.6	+41 24 48	7.13	0.99	0.62	0.22	0.46	–	–	1
181	J1930-1509	19 30 01.9	-15 09 19	7.25	0.99	10.01	1.48	0.85	0.08	15.58	1, 15
182	J1944+7815	19 44 11.2	+78 16 18	5.56	0.99	2.80	0.56	0.72	–	–	1
183	J1946+0201	19 46 4.40	+02 01 54	4.26	0.99	3.06	0.30	1.03	–	–	1
184	J1950-2817	19 50 45.9	-28 17 39	3.37	0.99	4.25	0.62	0.86	–	–	1
185	J2000-0101	20 00 52.7	-01 01 09	4.29	0.99	0.50	0.12	0.63	–	–	1, 6
186	J2015+1144	20 15 20.9	+11 44 49	2.97	0.99	0.49	0.13	0.59	–	–	1
187	J2042-0310	20 42 56.5	-03 10 22	6.48	0.99	0.49	0.16	0.50	0.14	2.32	1
188	J2049+3526	20 49 53.2	+35 26 52	8.08	0.99	0.44	0.11	0.62	–	–	1, 9
189	J2102-0921	21 02 15.7	-09 21 15	5.52	0.99	1.38	0.42	0.53	0.08	2.12	1
190	J2108+6049	21 08 41.1	+60 49 03	4.21	0.99	0.63	0.17	0.58	–	–	1, 8
191	J2111+3335	21 11 37.7	+33 35 12	8.49	0.99	0.63	0.11	0.78	–	–	1, 2
192	J2138+8307	21 38 49.8	+83 07 04	2.84	0.99	0.78	0.31	0.41	0.14	3.82	1, 2
193	J2139-3218	21 39 30.5	-32 18 38	5.00	0.83	0.94	0.24	0.61	–	–	1, 6
194	J2144+8015	21 44 0.71	+80 15 12	4.63	0.99	0.35	0.12	0.47	–	–	1, 4
195	J2144-3105	21 44 04.8	-31 05 18	1.71	0.98	0.49	0.11	0.66	0.18	4.27	1, 4
196	J2157+0037	21 57 31.4	+00 37 57	5.24	0.99	1.12	0.24	0.69	0.39 ^b	54.80	1, 6
197	J2158+6014	21 58 46.9	+60 14 41	5.03	0.99	0.51	0.09	0.77	–	–	1, 8
198	J2212+1304	22 12 54.4	+13 04 36	1.60	0.99	1.76	0.07	1.44	0.15	11.54	1
199	J2300+1426	23 00 47.4	+14 26 03	4.48	0.99	1.29	0.23	0.77	0.15 ^b	8.46	1
200	J2301-4333	23 01 17.7	-43 33 24	4.89	0.99	1.02	–	–	–	–	6, 14
201	J2310+0734	23 10 22.6	+07 34 53	9.33	0.99	0.62	0.04	1.22	0.04	0.03	1
202	J2322+4157	23 22 43.3	+41 58 14	7.32	0.99	1.09	0.39	0.46	0.11 ^a	3.82	1
203	J2348+0043	23 48 23.9	+00 43 47	1.17	0.99	0.66	0.09	0.89	0.36	28.63	1, 2, 11

1: NVSS (Condon et al. 1990); 2: VLSS (Cohen et al. 2007); 3: 4C (Pilkington & Scott 1965; Gower et al. 1967; Caswell & Crowther 1969); 4: 6C (Baan & McKee 1985; Hales et al. 1988, 1990, 1991, 1993a,b); 5: 7C (McGilchrist et al. 1990; Kollgaard et al. 1994; Waldram et al. 1996; Vessey & Green 1998); 6: PMN (Griffith et al. 1994); 7: PKS (Bolton et al. 1964); 8: 87GB (Gregory & Condon 1991); 9: B2 (Colla et al. 1970, 1972, 1973; Fanaroff & Riley 1974); 10: B3 (Ficarra et al. 1985); 11: VFK (van Velzen et al. 2015); 12: CRATES (Healey et al. 2007); 13: FIRST (Becker et al. 1995); 14: SUMSS (Mauch et al. 2003); 15: 2MASS (Skrutskie et al. 2006); 16: MG2 (Bennett et al. 1986); 17: MRC (Large et al. 1981); 18: SSTSLS (Randall et al. 2012)

- Huchra J. P. et al., 2012, ApJS, 199, 26
Intema H. T., Jagannathan P., Mooley K. P., Frail D. A., 2017, A&A, 598
Ishwara-Chandra C. H., Sirothia S. K., Wadadekar Y., et al. 2010, MNRAS, 405, 436
Jarrett T. H, Chester J., and Cutri R., 2000, ApJ, 119.5, 2498
Jones T. W., & Owen F. N. 1979, ApJ, 234, 818
Kapahi V. K., Athreya R. M., van Breugel W. et al., 1998, ApJS, 118, 275
Koester B. P. et al., 2007, ApJ, 660, 239
Khatri Rishi., 2016, A&A, 592, 48
Kollgaard R. I., Brinkmann W., Chester M. M., Feigelson E. D., Hertz P., Reich P., Wielebinski R., 1994, ApJS, 93, 145
Large M. I., Mills B. Y., Little A. G., Crawford D. F., Sutton J. M., 1981, MNRAS, 194, 693L
Leahy J. P., Williams A. G., 1984, MNRAS, 210, 929
Lopes P. A. A., de Carvalho R. R., Gal R. R., Djorgovski S. G., Odewahn S. C., Mahabal A. A., Brunner R. J., 2004, AJ, 128, 1017
Lumsden S. L., Nichol R. C., Collins C. A., Guzzo L., 1992, MNRAS, 258, 1
Massaro F., Capetti A., Paggi A., Baldi R. D., Tramacere A., Pilleri A. I., et al., 2020, Apjs, 247, 71
Malmquist K. G., 1922, Lund Medd. Ser. I, 100, 1
Malmquist K. G., 1936, Stockholms Obs. Medd., 26
Mguda Z., Faltenbacher A., van der Heyden K., Gottlöber S., Cress C., Vaisanen P., Yepes G., 2015, MNRAS, 446, 3310
Mahony, E. K., Morganti, R., Prandoni, I., et al. 2016b, MNRAS, 463, 2997
Mao M. Y., Sharp R., Saikia D. J., Norris R. P., Hollitt M. J., Middelberg E., Lovell J. E. J., 2010, MNRAS, 406, 2578
Mao M. Y., Johnston-Hollitt M., Stevens J. B., & Wotherspoon S. J., 2009, MNRAS, 392, 1070
Mauch T., Murphy T., Buttery H. J., Curran J., Hunstead R. W., Piestrzynski B., Robertson J. G., Sadler E. M., 2003, MNRAS, 342, 1117
McGlynn T. A. et al., 2004, ApJ, 616, 1284
McGilchrist M. M., Baldwin J. E., Riley J. M., Titterton D. J., Waldram E. M., Warner P. J., 1990, MNRAS, 246, 110
Miller Christopher J. et al., 2005, AJ, 130, 968
Miley G. K., Perola G. C., van der Kruit P. C., van der Laan H., 1972, Nature, 237, 269
Missaglia V., Massaro F., Capetti A., Paolillo M., Kraft R. P., Baldi R. D., and Paggi A., 2019, A&A, 626, A8
Mauch T., Sadler E. M., 2007, MNRAS, 375, 931
Moore B., Frenk C. S., and White S. D. M., 1993, MNRAS, 261, 827
O'Brien, A. N., Norris R. P., Tothill N. F. H. Filipović, M. D., MNRAS, 2018, 481, 4
O'Dea C.P., Owen F.N., 1985, AJ, 90, 927
O'Dea C.P., Owen F.N., 1986, AJ, 300, 841
O'Donghue A. A., Owen F., Eilek J.A., 1990, ApJS, 72, 75

Table 2. Candidate NAT radio sources

Cat No.	Name	R.A-core (J2000.0)	Dec-core (J2000.0)	Separation (arsec)	ρ	F_{150} (Jy)	F_{1400} (Jy)	$\alpha_{0.15}^{1.4}$ (± 0.05)	z	L_{150} WHz^{-1} $\times 10^{25}$	Other Catalog
(1)	(2)	(3)	(4)	(5)	(6)	(7)	(8)	(9)	(10)	(11)	(12)
1	J0003+5745	00 03 18.9	+57 45 28	7.33	0.99	0.43	0.16	0.44	—	—	8
2	J0041–0922	00 41 30.9	–09 22 33	7.23	0.99	10.5	—	—	—	—	17
3	J0041–4346	00 41 29.5	–43 47 05	4.27	0.99	0.73	—	—	—	—	18
4	J0102–0050	01 02 39.8	–00 50 41	2.32	0.99	0.43	0.13	0.53	—	—	1, 11
5	J0141+1623	01 41 35.5	+16 23 36	4.87	0.99	1.05	0.16	0.84	—	—	1, 8
6	J0148–3155	01 48 15.4	–31 55 20	3.23	0.99	0.73	0.08	0.97	0.14	9.42	1
7	J0223+4300	02 23 19.4	+42 59 47	4.72	0.99	20.1	5.56	0.57	0.02	17.88	10
8	J0228–2814	02 28 26.0	–28 14 13	4.14	0.99	3.45	0.68	0.72	0.20	17.38	1
9	J0236+1202	02 36 26.5	+12 02 51	1.14	0.93	0.49	0.06	0.94	—	—	1
10	J0303+6605	03 03 0.44	+66 05 43	4.45	0.99	2.38	0.33	0.88	—	—	1
11	J0303+1610	03 03 57.7	+16 10 41	5.77	0.99	0.74	0.29	0.41	—	—	1
12	J0335+6517	03 35 9.20	+65 17 04	1.10	0.81	0.38	0.20	0.28	—	—	1
13	J0411+6133	04 11 50.0	+61 33 10	1.72	0.99	1.18	0.23	0.73	—	—	1
14	J0516+3531	05 16 19.7	+35 31 49	4.09	0.99	0.46	0.12	0.60	—	—	1
15	J0523+2427	05 23 34.9	+24 27 27	10.1	0.98	0.96	0.20	0.70	—	—	9
16	J0541+2842	05 41 13.4	+28 42 47	10.7	0.91	7.24	1.40	0.73	—	—	1, 3
17	J0549–2520	05 49 21.6	–25 20 47	4.61	0.99	0.75	0.20	0.59	0.04	0.27	1, 2
18	J0603+5108	06 03 53.9	+51 08 29	7.33	0.99	1.28	0.21	0.80	—	—	1
19	J0603+5619	06 03 28.0	+56 19 29	9.14	0.99	6.36	0.01	1.74	—	—	1
20	J0704+6318	07 04 28.7	+63 18 39	4.43	0.99	6.67	0.03	2.04	0.09	14.87	1, 2
21	J0709+5100	07 09 53.2	+51 00 58	1.78	0.99	1.32	0.16	0.94	—	—	1, 8, 11
22	J0728–0008	07 28 50.3	–00 08 21	7.39	0.99	3.49	0.78	0.67	—	—	—
23	J0730+4051	07 30 43.3	+40 51 52	1.83	0.93	0.93	0.54	0.24	0.12 ^b	3.22	1, 11
24	J0735+2510	07 35 42.3	+25 10 16	10.6	0.96	2.08	0.23	0.98	—	—	1, 11
25	J0802+6345	08 02 02.5	+63 45 55	3.27	0.99	0.78	0.07	0.98	0.07 ^a	1.18	4, 11, 14
26	J0810–4923	08 10 42.6	–49 23 54	5.12	0.99	11.1	—	—	—	—	—
27	J0815+3710	08 15 45.6	+37 10 24	6.34	0.96	0.51	0.13	0.61	—	—	4
28	J0818–0004	08 19 0.50	–00 04 57	4.94	0.99	0.42	0.06	0.87	—	—	1
29	J0928+4854	09 28 22.1	+48 54 33	6.00	0.80	0.64	0.11	0.78	—	—	1, 4, 8
30	J0953+7057	09 53 59.7	+70 57 34	2.93	0.99	4.88	0.26	1.31	0.18 ^a	47.33	1, 4, 8
31	J1108–4823	11 08 51.0	–48 23 50	1.81	0.99	1.02	—	—	—	—	14
32	J1111+4050	11 11 39.7	+40 50 24	1.21	0.79	6.65	0.98	0.85	0.07 ^b	7.91	11, 13
33	J1122+2124	11 22 30.5	+21 24 45	3.46	0.99	2.91	0.62	0.69	0.16	19.75	11
34	J1146–5236	11 46 30.1	–52 36 39	4.91	0.99	1.23	—	—	—	—	6
35	J1202+8522	12 02 11.4	+85 22 18	3.95	0.99	0.61	0.13	0.69	—	—	1, 4
36	J1215–3905	12 15 18.6	–39 05 17	10.5	0.94	1.43	0.19	0.90	—	—	1, 6
37	J1236–3535	12 36 45.1	–35 35 14	0.75	0.99	0.81	0.09	0.98	0.07 ^b	—	1
38	J1240–3413	12 40 03.7	–34 13 29	10.7	0.99	0.89	—	—	0.07	—	1
39	J1255–4447	12 55 57.3	–44 47 54	5.12	0.92	0.53	—	—	—	—	14
40	J1259–4458	12 59 45.6	–44 58 37	3.21	0.99	4.29	—	—	—	—	7, 14
41	J1303+3150	13 03 15.5	+31 50 18	1.81	0.61	2.15	0.20	1.06	0.16	28.22	1, 2
42	J1306+4633	13 06 45.7	+46 33 29	3.89	0.99	3.24	0.21	1.22	0.22 ^b	48.89	1, 2
43	J1347–3905	13 47 39.3	–39 05 42	7.23	0.99	0.42	0.04	1.05	—	—	1
44	J1409+7753	14 09 26.0	+77 53 17	2.53	0.99	0.41	0.11	0.58	—	—	1
45	J1425+1210	14 25 15.2	+12 10 09	4.47	0.99	1.38	0.49	0.46	0.15	7.89	11, 17
46	J1629+0104	16 29 27.3	+01 04 07	1.14	0.99	1.91	0.31	0.81	—	—	1
47	J1657–0148	16 57 52.6	–01 48 01	5.88	0.99	1.97	0.07	1.49	—	—	1
48	J1710+4239	17 10 40.7	+42 39 45	6.94	0.99	1.54	0.46	0.54	—	—	1
49	J1924–0032	19 24 07.0	–00 32 07	6.94	0.99	1.05	0.21	0.72	—	—	1, 8
50	J1926+4831	19 26 09.5	+48 31 28	3.13	0.99	1.19	0.02	1.82	—	—	1, 4
51	J1930–0312	19 30 57.3	–03 12 56	8.96	0.99	0.80	0.22	0.57	—	—	1, 6
52	J2038–2011	20 38 27.7	–20 11 07	1.13	0.99	2.98	0.77	0.60	0.51	—	1
53	J2058–2125	20 58 03.8	–21 25 19	3.55	0.97	1.14	0.11	1.04	—	—	1

O’Donoghue A. A., Eilek J. A., Owen F. N., 1993, ApJ, 408, 428

Owen F. N., Rudnick L., 1976, ApJL, 205, L1

Owen F., Burns J., and Rudnick L., 1979, Ap. J. (Letters), 226, L1 19

Pan T., Yu H., van Weeren R. J., Jia S., Li C., and Lyu Y., 2021,

ApJS, 254, 30

Pal S. and Kumari S., 2021, arXiv:2103.15153

Pal S. and Kumari S., 2021a, arXiv:2103.15199

Patra D., Pal S., Konar C., Chakrabarti S. K., 2019, Astrophysics and Space Science, 72, 45

Table 2 – continued Candidate NAT radio sources

Cat N0.	Name	R.A-core (J2000.0)	Dec-core (J2000.0)	Separation (arsec)	ρ	F_{150} (Jy)	F_{1400} (Jy)	$\alpha_{0.15}^{1.4}$ (± 0.05)	z	L_{150} WHz^{-1} $\times 10^{25}$	Other Catalog
(1)	(2)	(3)	(4)	(5)	(6)	(7)	(8)	(9)	(10)	(11)	(12)
54	J2104+1916	21 04 21.4	+19 16 46	4.18	0.99	3.63	0.42	0.96	–	–	1, 3
55	J2137–4105	21 37 51.4	–41 05 19	7.31	0.99	2.19	–	–	0.06	–	14
56	J2144+2107	21 44 06.4	+21 07 44	2.87	0.99	0.38	0.16	0.38	–	–	1, 8
57	J2201–4427	22 01 58.5	–44 27 06	2.33	0.99	1.11	–	–	–	–	6, 14
58	J2227–3034	22 27 54.5	–30 34 32	2.17	0.99	3.83	0.89	0.65	0.06	0.75	1
59	J2319–1838	23 19 30.0	–18 38 05	6.12	0.99	0.45	0.15	0.49	–	–	1, 6
60	J2348–3117	23 48 54.9	–31 17 32	8.80	0.99	1.14	0.33	0.55	0.18	9.75	1
61	J2351+0033	23 51 54.4	+00 33 10	4.67	0.95	0.27	0.08	0.54	0.27	05.56	1,11

1: NVSS (Condon et al. 1990); 2: VLSS (Cohen et al. 2007); 3: 4C (Pilkington & Scott 1965; Gower et al. 1967; Caswell & Crowther 1969); 4: 6C (Baan & McKee 1985; Hales et al. 1988, 1990, 1991, 1993a,b); 5: 7C (McGilchrist et al. 1990; Kollgaard et al. 1994; Waldram et al. 1996; Vessey & Green 1998); 6: PMN (Griffith et al. 1994); 7: PKS (Bolton et al. 1964); 8: 87GB (Gregory & Condon 1991); 9: B2 (Colla et al. 1970, 1972, 1973; Fanaroff & Riley 1974); 10: B3 (Ficarra et al. 1985); 11: VFK (van Velzen et al. 2015); 12: CRATES (Healey et al. 2007); 13: FIRST (Becker et al. 1995); 14: SUMSS (Mauch et al. 2003); 15: 2MASS (Skrutskie et al. 2006); 16: MG2 (Bennett et al. 1986); 17: MRC (Large et al. 1981); 18: SSTSL (Randall et al. 2012)

^a presents photometric redshift

^b presents spectroscopic redshift

- Piffaretti R., Arnaud M., Pratt G. W., Pointecouteau E., Melin J. B., 2011, *A&A*, 534, 109
- Pinkney J., Burns J. O., Rhee G., Hill J. M., 1998, *AJ*, 108, 2031
- Pinkney J., Burns J. O., Rhee G., Hill J. M., 1992, *BAAS*, 24, 193
- Pilkington J. D. H., Scott J. F., 1965, *MNRAS*, 69, 183
- Prestage R. M., and Peacock J. A. 1988, *MNRAS*, 230, 131
- Proctor D. D., 2011, *ApJS*, 194, 31
- Proctor D. D., 2016, *ApJS*, 224, 18
- Quintana H., Lawrie D. G., 1982, *AJ*, 87, 1
- Randall K. E., Hopkins A. M., Norris R. P., Zinn P. -C., Middelberg E., Mao M. Y., Sharp R. G., 2012, *MNRAS*, 421, 1644R
- Richter G. A. 1975, *Astron. Nachr.*, 296, 65
- Rozo E., Rykoff E. S., Becker M., Reddick R. M., Wechsler R. H., 2015, *MNRAS*, 453, 38
- Ryle M., and Windram, M. D. 1968, *MNRAS*, 138, 1
- Shimwell T.W. et al., 2019, *A&A*, 622, A1
- Sakelliou I., Merrifield M. R. 2000, *MNRAS*, 311, 649
- Sebastian B. , Lal, D. V., Rao. A., 2017, *AJ*, 154, 169
- Skrutskie M. F. et al., 2006, *AJ*, 131, 1163
- Skrutskie M. F., Cutri R. M., Stiening R., et al. 2006, *AJ*, 131, 1163
- Srivastava S., Singal A. K., 2020, *MNRAS*, 493, 3811
- Smith D. J. B., et al., 2011, *MNRAS*, 416, 857
- Smith Anthony G., Hopkins Andrew M., Hunstead Richard W., Pimblet Kevin A., 2012, *MNRAS*, 422, 25
- Smolcic V. et al. 2007, *ApJS*, 172, 295
- Stocke J. 1977, Ph.D. dissertation, University of Arizona, unpublished
- Sun M., Jerius D., and Jones C., 2005, *AJ*, 633, 165
- Sutherland W. and Saunders W., 1992, *MNRAS*, 259, 413
- Swarup G. et al., 1991, *Current Science*, 60, 95.
- Tasse C., Best P. N., Röttgering H., and Le Borgne D., 2008, *A&A*, 490, 893
- Terni de Gregory B. et al., 2017, *A&A*, 608, A58
- Vallee J. P., Bridle A. H., Wilson A. S., 1981, *Astrophys. J.*, 250, 66
- Van Velzen S., Falcke H., KÖrding E., 2015, *MNRAS*, 446, 2985
- Vessey S. J., Green D. A., 1998, *MNRAS*, 294, 607
- Waldram E. M., Yates J. A., Riley J. M., Warner P. J., 1996, *MNRAS*, 282, 779
- Wen Z. L., Han J. L., Liu F. S., 2012, *ApJS*, 199, 34
- Wen Z. L., Han J. L., 2015, *ApJ*, 807, 178
- Wetzel A. R., Tinker J. L., and Conroy C., 2012, *MNRAS*, 424, 232
- White R.A., Bliton M., Bhavsar S.P., Bornmann P., Burns J.O., Ledlow M.J., Loken C., 1999, *AJ*, 118, 2014
- Wing J. D., Blanton E. I., 2011, *AJ*, 141, 88
- Worrall D. M. and Birkinshaw M. 2000, *ApJ*, 530, 719
- Xu C., O’dea C. P., Biretta J. A., 1999, *AJ*, 117, 2026
- Yoon Joo H., Schawinski Kevin., Sheen Yun-Kyeong., Ree Chang H., Yi Sukyoung K., 2008, *ApJS*, 176, 414
- Yu-Xing Liu, Hai-Guang Xu, Dong-Chao Zheng, Wei-Tian Li, Zheng-Hao Zhu, Zhi-Xian Ma, and Xiao-Li Lian, 2019, *RAA*, 19, 127
- Zwicky F., Herzog E., Wild P., Karpowicz M., Kowal C. T., 1961, Pasadena: California Institute of Technology (CIT)
- Williams W. L., Hardcastle M. J., Best P. N., et al. 2019, *A&A*, 622, A2
- Wright E. L., et al., 2010, *AJ*, 140, 1868

This paper has been typeset from a $\text{\TeX}/\text{\LaTeX}$ file prepared by the author.

Table 3. Cluster details for candidate WAT radio source.

Cat No	Name	Cluster	z_{cl}	(D_c) (Mpc)	θ ($''$)	D (kpc)	m_r	r_{500} (Mpc)	R_L	N_{500}	M_{500} $\times 10^{14} M_\odot$	ρ_{co} (Mpc^{-3})
1.	J0003-3556	ABELL 2717	0.05	218.4	036.9	133.8	–	–	–	–	–	–
2.	J0022+2317	RM J002224.7+231733.0	0.13	556.6	04.8	41.2	–	–	–	–	–	–
3.	J0030+1058	NSC J003033+105852	–	–	78.0	–	–	–	–	–	–	–
4.	J0054+3339	ZwCl 0051.7+3322	–	–	222.0	–	–	–	–	–	–	–
5.	J0114+0029	WHL J011425.6+002933	0.34	1377	00.6	10.7	18.36	0.82	39.20	19	2.25	53.0
6.	J0120+1451	YSS2008 466	0.05	218.4	162.0	586.7	–	–	–	–	–	–
7.	J0123+3315	MCXC J0123.6+3315	0.02	88.0	021.6	31.6	–	–	–	–	–	–
8.	J0128+3448	WHL J012859.1+344842	0.15	639.0	000.1	0.96	16.32	0.88	35.48	21	2.01	58.6
9.	J0149+1403	MSPM 01728	0.07	304.3	003.6	17.8	–	–	–	–	–	–
10.	J0204+0415	WHL J020431.3+041501	0.14	597.9	038.4	350.7	16.2	0.60	14.9	9	0.87	25.1
11.	J0205-4124	SPT-CL J0205-4125	–	–	258.0	–	–	–	–	–	–	–
12.	J0209+0950	NSC J020939+094834	0.09	389.3	138.0	859.1	–	–	–	–	–	–
13.	J0257-0400	WHL J025743.7-035951	0.18	760.8	010.8	121.3	18.9	0.80	31.8	19	2.00	53.0
14.	J0306-1206	ABELL 0415	0.08	346.9	294.0	1643.0	–	–	–	–	–	–
15.	J0315+0507	WHL J031530.6+050746	0.22	920.2	006.0	78.9	17.3	0.69	17.5	9	1.04	25.1
16.	J0317+1212	WHL J031723.6+121234	0.22	920.2	006.0	78.9	16.4	1.01	53.5	16	3.55	44.7
17.	J0522+2807	WHL J052246.0+280640	0.13	556.6	019.2	164.7	14.7	0.89	39.6	16	2.55	44.7
18.	J0631+2500	PSZ2 G188.38+07.05	0.08	346.9	055.8	311.8	–	–	–	–	–	–
19.	J0708+7152	WHL J070819.0+715224	0.11	473.4	067.8	503.9	15.3	–	57.2	–	3.49	–
20.	J0733+4211	WHL J073312.6+421156	0.48	1870.5	006.0	132.2	19.0	0.85	12.5	18	0.62	6.44
21.	J0736+2412	WHL J073618.1+241043	0.14	597.9	107.0	977.4	16.2	0.75	29.9	16	1.87	44.7
22.	J0757+3640	WHL J075753.2+364022	0.12	515.1	003.0	24.1	15.6	0.70	17.6	16	1.04	44.7
23.	J0805+1614	WHL J080543.1+161356	0.10	431.4	005.4	36.9	15.8	0.76	21.7	14	1.31	39.1
24.	J0818+5437	WHL J081803.9+543709	0.10	431.4	018.0	123.0	14.9	1.01	56.8	29	3.79	81.0
25.	J0856+4829	WHL J085600.8+482910	0.12	515.1	010.2	81.8	15.8	0.95	44.3	25	2.89	69.8
26.	J0912+1600	NSC J091232+155800	0.19	801.0	120.0	1409.0	–	–	–	–	–	–
27.	J0917+5509	WHL J091708.0+550908	0.19	801.0	000.2	2.4	16.27	0.79	33.56	15	1.89	41.9
28.	J0944+0247	WHL J094443.2+024754	0.21	880.7	000.4	5.07	16.59	1.12	91.99	46	5.62	128.5
29.	J1012+0841	WHL J101206.4+084133	0.09	389.3	000.2	1.3	15.78	0.65	11.72	10	0.52	27.93
30.	J1015+1221	WHL J101540.7+122030	0.61	2292.6	031.2	774.8	20.4	0.70	28.7	8	1.79	22.3
31.	J1019+7020	WHL J101956.5+702034	0.24	–	053.4	–	17.4	–	70.1	–	4.37	–
32.	J1022+5006	WHL J102228.4+500620	0.15	639.0	000.1	0.9	15.27	1.32	119.33	74	7.46	206.7
33.	J1032+3151	WHL J103214.4+315214	0.35	1413.6	054.6	996.9	17.8	1.00	55.4	26	3.69	72.6
34.	J1034+0736	WHL J103409.1+073616	0.45	1768.2	013.2	280.8	–	–	–	–	–	–
35.	J1042+0237	NSC J104200+023739	0.04	175.2	004.2	12.3	–	–	–	–	–	–
36.	J1046-2911	ABELL S0646	0.06	261.5	019.8	85.0	14.31	–	17.2	–	0.93	–
37.	J1048+3532	RM J104851.5+353136.4	0.36	1450.0	039.0	725.4	19.1	–	–	–	–	–
38.	J1050+0432	MaxBCG J162.734+4.525	0.12	515.1	081.6	654.5	–	–	–	–	–	–
39.	J1050-2405	MCXC J1050.6-2405	0.20	840.9	026.4	322.4	–	–	–	–	–	–
40.	J1051+1825	NSC J105152+182302	0.11	473.4	180.0	1338.0	–	–	–	–	–	–
41.	J1056+0255	WHL J105617.0+025526	0.39	1558.0	000.1	1.9	18.92	0.70	27.38	14	1.52	39.1
42.	J1058+0136	SDSS-C4 1110	0.04	175.2	053.4	156.7	13.6	–	28.9	–	1.64	–
43.	J1118+2754	NSC J111853+275216	0.06	261.5	132.0	566.9	–	–	–	–	–	–
44.	J1119+6317	WHL J111933.1+631717	0.16	679.8	000.6	6.1	15.68	0.76	26.27	16	1.45	44.7
45.	J1120+2912	WHL J112038.5+291234	0.27	1114.4	002.2	33.1	17.0	0.73	21.0	11	1.27	30.7
46.	J1130+2524	WHL J113048.8+252436	0.15	639.0	001.8	17.4	16.2	0.71	20.5	16	1.23	44.7
47.	J1132+6311	NSC J113242+631204	0.10	431.4	060.6	414.2	–	–	–	–	–	–
48.	J1142+1102	WHL J114254.3+110133	0.15	639.0	033.0	325.5	16.0	1.13	82.6	46	5.37	128.5
49.	J1151+0422	NSC J115145+042203	0.13	556.6	000.4	3.4	–	–	–	–	–	–
50.	J1155+5755	WHL J115556.3+575501	0.16	679.8	029.4	300.2	16.5	0.84	28.0	18	1.74	50.2
51.	J1156+3432	GMBCG J179.0225+34.55	0.26	1076.0	029.4	437.9	1.52	–	–	–	–	–
52.	J1202+5802	WHL J120203.8+580207	0.09	389.3	001.0	6.2	15.2	0.94	46.1	30	3.02	83.8
53.	J1205+3204	WHL J120514.5+320417	0.17	720.4	000.2	2.2	16.52	0.87	–	–	–	–
54.	J1206+3152	WHL J120647.7+315231	0.15	639.0	000.6	5.8	16.90	0.77	29.65	14	1.65	39.1
55.	J1242+5021	WHL J124207.4+502147	0.15	639.0	000.4	3.8	16.33	0.52	10.28	5	0.53	13.96
56.	J1249+0144	WHL J124943.7+014447	0.20	840.9	031.4	383.4	16.9	0.98	52.8	38	1.50	106.1
57.	J1304+6439	WHL J130428.8+643937	0.23	959.4	001.0	13.6	16.3	0.79	29.3	13	1.83	36.3
58.	J1307+5651	MaxBCGJ196.932+56.850	0.23	959.4	000.3	4.1	–	–	–	–	–	–
59.	J1311-0120	WHL J131132.1-011946	0.17	720.4	015.0	161.0	–	–	–	–	–	–
60.	J1315+4841	WHL J131527.6+484025	0.48	1870.5	056.8	1252.0	19.8	1.03	81.9	39	5.68	108.9

Table 3 – *continued* Cluster details for candidate WAT radio source.

Cat No	Name	Cluster	z_{cl}	(D_c) (Mpc)	θ (")	D (kpc)	m_r	r_{500} (Mpc)	R_L	N_{500}	M_{500} $\times 10^{14} M_\odot$	ρ_{co} (Mpc^{-3})
61.	J1321+4235	MSPM 05039	0.08	346.9	083.5	468.0	–	–	–	–	–	–
62.	J1325+5736	WHL J132511.2+573601	0.12	515.1	006.6	52.9	14.1	1.03	109.4	59	7.81	164.8
63.	J1331–0544	ABELL 1751	0.15	642.8	090.0	243.7	16.2	–	34.2	–	1.98	–
64.	J1412+7420	ABELL 1893	0.21	880.7	133.2	1689.0	–	–	–	–	–	–
65.	J1414+0143	MSPM 01989	0.05	218.4	079.0	286.1	–	–	–	–	–	–
66.	J1416+0219	NSC J141606+021843	0.15	639.0	108.1	1046.8	–	–	–	–	–	–
67.	J1440+0328	WBL 518	0.02	88.0	012.1	18.0	–	–	–	–	–	–
68.	J1449+3959	WHL J144900.9+400044	0.19	801.0	084.0	986.3	16.8	0.66	18.5	13	1.10	36.3
69.	J1450+4418	WHL J145039.8+441829	0.27	1114.4	003.6	55.1	17.5	1.02	73.1	36	5.01	100.5
70.	J1509+3327	WHL J150959.8+332746	0.11	473.4	001.2	10.1	–	–	–	–	–	–
71.	J1553+1530	ZwCl 1551.4+1539	0.14	597.9	001.0	10.2	–	–	–	–	–	–
72.	J1604+2355	WHL J160456.7+235558	0.05	218.4	001.3	5.6	12.7	–	15.0	–	0.80	–
73.	J1612+2929	MSPM 00091	0.03	131.7	083.0	184.1	–	–	–	–	–	–
74.	J1615+4711	WHL J161541.3+471004	0.20	840.9	104.6	1278.8	17.0	0.83	33.3	20	2.11	55.8
75.	J1616+0926	WHL J161653.2+092635	0.20	840.9	000.8	9.8	–	–	–	–	–	–
76.	J1636+2718	WHL J163604.2+271829	0.13	556.6	014.4	123.5	15.7	0.74	22.4	14	1.36	39.1
77.	J1711+1351	WHL J171150.9+135151	0.23	959.4	001.0	13.6	16.1	0.83	33.6	12	2.13	33.5
78.	J1717+3734	WHL J171725.4+373458	0.09	389.3	000.6	3.7	–	–	–	–	–	–
79.	J1735+3137	RM J173507.0+313755.5	0.26	1076.0	007.5	130.3	17.8	–	26.8	–	2.33	–
80.	J1930–1509	MCXC J1930.0-1509	0.08	346.9	026.3	147.4	14.4	–	32.7	–	1.88	–
81.	J2138+8307	ABELL 2387	0.14	597.9	029.3	268.1	–	–	–	–	–	–
82.	J2139–3218	APMCC 693	0.08	348.9	105.8	165.6	17.0	–	39.6	–	2.33	–
83.	J2144–3105	EDCC 027	0.18	765.4	114.4	196.7	16.9	–	31.1	–	1.78	–
84.	J2212+1304	MaxBCG J333.226+13.076	0.15	639.0	000.1	0.96	–	–	–	–	–	–
85.	J2226+1721	ABELL 2443	0.11	473.4	062.6	465.3	14.9	–	52.5	–	3.18	–
86.	J2300+1426	WHL J230046.8+142602	0.15	639.0	001.2	10.6	–	–	–	–	–	–
87.	J2310+0734	Pegasus II CLUSTER	0.04	75.2	058.0	12.0	13.3	–	45.8	–	2.73	–
88.	J2322+4157	ZwCl 2322.4+4157.6	–	–	486.0	–	–	–	–	–	–	–
89.	J2348+0043	SDSS CE J357.08+00.73	0.39	1558.0	061.0	1192.7	–	–	–	–	–	–

Table 4. Cluster details for candidate NAT radio source.

Cat No	Name	Cluster	z_{cl}	(D_c) (Mpc)	θ ($''$)	D (kpc)	m_r	r_{500} (Mpc)	R_L	N_{500}	M_{500} $\times 10^{14} M_\odot$	ρ_{co} (Mpc^{-3})
1.	J0013-1930	WHY J001334.0-192902	0.09	389.3	132.6	826.1	15.1	–	92.5	–	6.49	–
2.	J0041-0922	ABELL 0085	0.05	218.4	108.6	394.0	–	–	–	–	–	–
3.	J0041-4346	ABELL 2809	0.15	639.0	190.8	1849.4	15.9	–	23.0	–	1.28	–
4.	J0102-0050	NSCS J010240-005003	0.25	1037.3	041.4	599.1	17.5	–	34.6	–	–	–
5.	J0148-3155	ABELL 2943	0.14	597.9	016.8	153.4	16.3	–	88.3	–	5.63	–
6.	J0228-2814	ABELL 3023	0.21	880.7	067.2	852.5	–	–	–	–	–	–
7.	J0653+6919	RX J0653.4+6919	0.15	639.0	069.0	668.8	–	–	–	–	–	–
8.	J0704+6318	ABELL 0556	0.09	389.3	034.2	212.9	15.1	–	82.2	–	5.20	–
9.	J0730+4051	WHL J073045.4+405038	0.12	515.1	060.0	481.2	–	–	–	–	–	–
10.	J0735+2510	WHL J073539.8+251020	0.08	346.9	048.0	269.0	14.9	0.88	37.2	18	2.38	50.2
11.	J0802+6345	NSC J080155+634523	0.09	389.3	053.4	332.4	–	–	–	–	–	–
12.	J0953+7057	ABELL 0875	0.18	760.8	136.6	1534.7	16.2	–	38.5	–	2.26	–
13.	J1038-2453	PSZ2 G268.30+28.89	0.12	515.1	054.2	434.7	15.4	–	–	–	–	–
14.	J1111+4050	ABELL 1190	0.07	304.3	067.8	336.0	–	–	–	–	–	–
15.	J1122+2124	WHL J112229.9+212422	0.15	639.0	022.8	221.0	16.4	1.16	83.7	45	5.82	125.7
16.	J1236-3535	ABELLs 0701	0.07	304.3	196.2	972.4	14.4	–	33.2	–	1.92	–
17.	J1240-3413	ABELL 3524	0.07	304.3	020.4	101.1	14.0	–	32.7	–	1.89	–
18.	J1303+3150	ABELL 4056	0.21	880.7	267.2	–	–	–	–	–	–	–
19.	J1306+4633	WHL J130650.0+463333	0.24	998.5	044.4	623.3	16.1	1.41	165.7	87	12.33	243.0
20.	J1314+6220	NSC J131425+621907	0.13	556.6	036.6	314.1	–	–	–	–	–	–
21.	J1409+7753	NSC J140833+775227	0.19	801.0	108.6	1275.1	–	–	–	–	–	–
22.	J1425+1210	NSC J142513+120946	0.15	639.0	038.4	372.2	–	–	–	–	–	–
23.	J1446-0846	ABELL 1964	0.07	304.3	168.0	832.6	–	–	–	–	–	–
24.	J1657-0148	RXSC J1657-0148	0.03	131.7	040.8	90.5	–	–	–	–	–	–
25.	J1710+4239	WHL J171040.7+423945	0.17	720.4	014.4	154.5	16.2	0.73	26.0	17	1.60	47.5
26.	J1926+4831	CIZA J1926.1+4833	0.09	389.3	067.2	418.3	15.3	–	58.0	–	3.54	–
27.	J2022-2056	ABELLs 0868	0.05	218.4	034.8	126.0	–	–	–	–	–	–
28.	J2137-4105	APMCC 688	0.06	261.5	252.0	1082.4	–	–	–	–	–	–
29.	J2227-3034	2PIGG J2227.0-3041	0.07	304.3	002.4	11.8	–	–	–	–	–	–
30.	J2348-3117	ABELL 4043	0.18	760.8	044.0	494.3	16.4	–	66.5	–	4.12	–
31.	J1930-0312	ABELL 3036	–	–	329.0	–	–	–	–	–	–	–

Table 5. Details of various cluster surveys used in the present work. The brief name is used to refer to the catalogues mentioned in this article. N is the number of clusters within the TGSS field without redshift, N_z is the number of those clusters with redshifts and N_t is the total number of cluster.

Sl No	Catalogue name	Observation band	N_z	N	N_t	ref.
1.	ABELL	Optical	7	–	7	Abell et al. (1989)
2.	RM	Optical, IR	3	–	3	Rozo et al. (2015)
3.	NSCS	Optical	2	–	2	Lopes et al. (2004)
4.	WHL	Optical, X ray	53	–	53	Wen et al. (2015)
5.	ZwCl	Optical	1	2	3	Zwicky et al. (1961)
6.	MCXC	X ray	3	–	3	Piffaretti et al. (2011)
7.	MSPM	Optical	4	–	4	Smith et al. (2012)
8.	SPT-CL	SZ	–	1	1	Bleem et al. (2015)
9.	CIZA	X ray	1	–	1	Ebeling et al. (2002)
10.	NSC	Optical	8	1	9	Gal et al. (2009)
11.	SDSS-C4	Optical	1	–	1	Miller et al. (2005)
12.	MaxBCG	Optical	3	–	3	Koester et al. (2007)
13.	GMBCG	Optical	1	–	1	Hao et al. (2010)
14.	APMCC	Optical	2	–	1	Dalton et al. (1997)
15.	EDCC	Optical	1	–	1	Lumsden et al. (1992)
16.	Pegasus	Optical	1	–	1	Chincarini et al. (1976)
17.	RX	X ray	1	–	1	McGlynn et al. (2004)
18.	2PIGG	IR	1	–	1	Eke et al. (2004)
19.	YSS	Optical	1	–	1	Yoon et al. (2008)
20.	PSZ2	Radio	2	–	2	Khatri et al. (2016)
21.	RXSC	X ray	1	–	1	Chon, Bohringer & Nowak (2013)
22.	WBL	Optical	1	–	1	White et al. (1999)